

DEFECTED GROUND STRUCTURE AND ITS APPLICATIONS
TO MICROWAVE DEVICES AND ANTENNA FEED
NETWORKS

A THESIS SUBMITTED TO
THE GRADUATE SCHOOL OF NATURAL AND APPLIED
SCIENCES
OF
MIDDLE EAST TECHNICAL UNIVERSITY

BY

ÖZGEHAN KILIÇ

IN PARTIAL FULFILMENT OF THE REQUIREMENTS
FOR
THE DEGREE OF MASTER OF SCIENCE
IN
ELECTRICAL AND ELECTRONICS ENGINEERING

SEPTEMBER 2010

Approval of the Thesis:

**DEFECTED GROUND STRUCTURE AND ITS
APPLICATIONS TO MICROWAVE DEVICES AND
ANTENNA FEED NETWORKS**

submitted by **ÖZGEHAN KILIÇ** in partial fulfillment of the requirements for the degree of **Master of Science in Electrical and Electronics Engineering Department, Middle East Technical University** by,

Prof. Dr. Canan Özgen
Dean, Graduate School of **Natural and Applied Sciences** _____

Prof. Dr. İsmet Erkmen
Head of Department, **Electrical and Electronics Eng.** _____

Assoc. Prof. Dr. Şimşek Demir
Supervisor, **Electrical and Electronics Eng. Dept., METU** _____

Examining Committee Members:

Prof. Dr. Gülbin Dural
Electrical and Electronics Eng. Dept., METU _____

Assoc. Prof. Dr. Şimşek Demir
Electrical and Electronics Eng. Dept., METU _____

Assoc. Prof. Dr. Özlem Aydın Çivi
Electrical and Electronics Eng. Dept., METU _____

Asst. Prof. Dr. Lale Alatan
Electrical and Electronics Eng. Dept., METU _____

Mehmet Erim İnal, M.Sc.
Aselsan A.Ş. _____

Date: 03.09.2010

I hereby declare that all information in this document has been obtained and presented in accordance with academic rules and ethical conduct. I also declare that, as required by these rules and conduct, I have fully cited and referenced all material and results that are not original to this work.

Name, Last Name : Özgehan Kılıç

Signature :

ABSTRACT

DEFECTED GROUND STRUCTURE AND ITS APPLICATIONS TO MICROWAVE DEVICES AND ANTENNA FEED NETWORKS

Kılıç, Özgehan

M.Sc., Department of Electrical and Electronics Engineering

Supervisor: Assoc. Prof. Dr. Şimşek Demir

September 2010, 74 pages

This thesis reports the analysis of the rectangular shaped defected ground structure (RS-DGS) and the application of the structure on some microwave devices. DGS is analyzed in terms of its superior properties, which enables the designers to easily realize many kind of microwave devices which are impossible to achieve with the standard applications. Within the scope of this thesis, the focus is on the rectangular shaped DGS and its characteristic properties. The basic slow wave and high impedance characteristics are utilized in the design of some microwave devices. The design is carried on at the two different frequency bands: X-band and K_a band, centering at 10 GHz and 35 GHz, respectively. Finally, using the high impedance property and the coupling between the defects, a wide band 1 : 4 beam forming network is designed and implemented at 10 GHz.

Keywords: Defected Ground Structure (DGS), impedance matching, high impedance, beam forming network (BFN), aperture coupling, unequal power divider.

ÖZ

KUSURLU TOPRAKLI YAPILAR VE MİKRODALGA AYGITLARDA VE ANTEN BESLEME AĞLARINDA UYGULAMALARI

Kılıç, Özgehan

Yüksek Lisans, Elektrik ve Elektronik Mühendisliği Bölümü

Tez Yöneticisi: Assoc. Prof. Dr. Şimşek Demir

Eylül 2010, 74 sayfa

Bu tez çalışmasında kusurlu topraklı yapılar ve bu yapıların mikrodalga aletlere uygulamaları incelenmiştir. Kusurlu topraklı yapılar standart uygulamalarla başarılması imkansız olan mikrodalga aygıtları kolayca gerçekleştirmeye izin veren üstün özellikleri açısından incelenmektedir. Bu tezin içeriğinde, odak dikdörtgen şekilli kusurlu topraklı yapı ve onun belirleyici özelliklerindedir. Temel yavaş dalga ve yüksek empedans özellikleri bazı mikrodalga aletlerin tasarımında kullanılmaktadır. Tasarım X bantı ve K_a bantı olmak üzere, 10 GHz ve 35 GHz merkezli iki farklı frekans bandında sürdürülmüştür. Sonuç olarak, yüksek empedans özelliği ve kusurlar arasındaki bağlaşımı kullanarak geniş bantlı 1 : 4 bir yapı 10 GHz’de tasarlanmış ve uygulanmıştır.

Anahtar Kelimeler: Kusurlu topraklı yapılar, empedans uyumlama, yüksek empedans, ışınım kurma ağı, açıklık bağlaşımı, eşitsiz güç bölücü.

To My Family

ACKNOWLEDGEMENTS

First and foremost, I would like to present my deepest appreciation and gratitude to my supervisor Şimşek Demir for his guidance and all the possibilities and opportunities he has provided me with throughout my undergraduate and graduate life. I am more than glad to have found the chance to work with him.

I would like thank Ozan Doğan Gürbüz, Caner Güçlü, and Ramazan Çetin for their support and companionship during the whole master period.

Then, I would like to thank all the former and current members and staff of METU RF Research Group for furnishing the best possible working environment with their fellowship and support because after some point way past the limit of weariness, this was one of the few things that kept me going, and I believe the case holds at least for most, if not all people in this research group.

Last but not the least, I would like to thank members of my family, my friends Andaç, Anıl, Birkal, Zülfükar, Şerife, Yiğit Yürek, Seda, and Yunus for their exceptional support, encouragement, help, and unparalleled patience with me during this study and my entire life.

Lastly, I'm pleased to acknowledge TUBITAK for its financial support during the whole Master's period (Project No. 104E048).

TABLE OF CONTENTS

ABSTRACT.....	iv
ÖZ	v
ACKNOWLEDGEMENTS	vii
TABLE OF CONTENTS.....	viii
LIST OF TABLES.....	ix
LIST OF FIGURES	x
CHAPTERS	
1. INTRODUCTION	1
2. DGS ANALYSIS.....	4
2.1 Literature Review.....	4
2.2 The Rectangular-Shaped Defected Ground Structure (RS-DGS) Analysis.....	6
3. POWER DIVIDER	16
3.1 T-junction.....	16
3.1.1 Equal Division T-Junction	16
3.1.2 Unequal Division T-Junction	23
3.1.3 Addition of Second Dielectric Under the DGS Layer	25
3.2 Aperture-Coupled Unequal Power Divider.....	27
3.2.1 Power Efficiency Examination	31
4. BEAM FORMING NETWORK.....	33
4.1 DGS 1 : 4 BFN Design	33
4.1.1 Addition of Dielectric Beneath the DGS	38
4.1.2 Implementation of the DGS 1 : 4 BFN	46
4.2 DGS 1 : 8 BFN Design	53
4.2.1 Addition of Dielectric Beneath the DGS	55
4.3 BFN at Millimeter-wave Frequencies.....	58
5. CONCLUSIONS	68
5.1 Future Work.....	69
REFERENCES	71

LIST OF TABLES

TABLES

Table 1. Defect Width Effect to Unequal Division for the Constant Defect Width at the 2 nd Port, 1.15 mm.	25
Table 2. Comparative Substrate Properties.....	58
Table 3. Power Division Ratios.	31

LIST OF FIGURES

FIGURES

Figure 1. Defected Ground Structure for Microstrip Line.....	2
Figure 2. Dumb-bell Shaped DGS.....	5
Figure 3.a. RS-DGS in the Form of a Transmission Line.....	7
Figure 4.a. Smith Chart Location of the RS-DGS with 2.65 mm Defect Width Normalized to 50 Ω Port Impedance.	8
Figure 5.a. Smith Chart Location of the RS-DGS with 2.65 mm Defect Width Normalized to 100 Ω Port Impedance.	8
Figure 6. Line Impedance versus Defect Width.	10
Figure 7. Line Impedance versus Line Width.....	11
Figure 8.a. S-parameters of the 100 Ω -Line-Impedance RS-DGS with 50 Ω Port Impedance.....	12
Figure 9. RS-DGS with Varying Length Defect.....	13
Figure 10.a. S_{11} for the RS-DGS with $w_d=2.65$, $l=3, 6, 9$ mm.....	14
Figure 11. Standard Microstrip T-junction.	17
Figure 12. T-junction with RS-DGS Matching Section.....	18
Figure 13. Results for the RS-DGS T-junction with $d=0$, $l=4.4$, $w_d=1.45$ mm.....	19
Figure 14.a. S_{11} for $l=3$, $d=0.2$, $w_d=1.4:0.2:2.2$ mm.....	20
Figure 15.a. S_{11} for $l=2$, $d=1$, $w_d=2.1:0.1:2.5$ mm.	21
Figure 16. S_{11} for $l=2.5 : 0.1 : 3.2$, $d=0.5$, $w_d=2$ mm.....	22
Figure 17.a. S_{11} for $l=2.7$, $d=0.5$, $w_{d2}=2.45 : 0.2 : 3.25$ mm.	24
Figure 18. Schematic View of a Dielectric-Added DGS.....	26

Figure 19. S-parameters for the Dielectric-Added DGS with Parameters $l=2.7$, $d=0.5$, $w_d=2$ mm.....	27
Figure 24. Standard 1 : 8 BFN.....	33
Figure 25. RS-DGS 1 : 4 Divider Structure.....	34
Figure 26.a. S_{11} of RS-DGS 1 : 4 Divider Structure for $d=0.5$, $w_d=2$, $l=2 : 0.4 : 2.8$ mm.	34
Figure 27.a. S_{11} for Varying Defect Width at $d=0.5$, $l = 2$ mm.....	35
Figure 28. S-parameters of the 1 : 4 Divider with $w_d=1.6$, $w_{d2}=w_{d5}=1.7$, $w_{d3}=w_{d4}=1.5$, $l=3$, $d=0.5$ mm.....	37
Figure 29. The Transmission Phase Characteristics in Degrees.	37
Figure 30. DGS 1 : 4 BFN.	39
Figure 31.a. S_{11} for 1 : 4 Divider with $l = 3$, $w_d = 1.4 : 0.2 : 1.8$ mm ($w_d=w_{d2}-0.1=w_{d3}+0.1$).	39
Figure 32.a. S_{11} for 1 : 4 Divider with $l = 3$, $w_d = 1.6$, $w_{d3} = 1.5, 1.7$ mm ($w_{d2}=w_{d3}+0.2$).	40
Figure 33.a. S_{11} for 1 : 4 Divider with $l = 3$, $w_d = 1.4 : 0.2 : 1.8$ mm ($w_d=w_{d2}-0.1=w_{d3}+0.1$) After the Addition of the Second Ground.....	41
Figure 34.a. S-parameters for the Resulting 1 : 4 BFN with 10 mm Distance between Ports ($l=3$, $d=0.5$, $w=1.15$, $w_d=1.8$, $w_{d2}=1.95$, $w_{d3}=1.65$ mm).	43
Figure 35.a. S-parameter Magnitude Values for the Resulting 1 : 4 BFN with 21 mm Spacing ($0.7*\lambda_0$) Between Two Ports ($w=1.15$, $l=3$, $d=0.5$, $l_0=21$, $w_d=1.8$, $w_{d2}=w_{d5}=2$, $w_{d3}=w_{d4}=1.6$ mm).....	44
Figure 36.a. The Implemented DGS 1 : 4 BFN.	46
Figure 37. a. The Implemented DGS 1 : 4 BFN in ADS Momentum.....	48
Figure 38. Measurement Results of the DGS 1 : 4 BFN.....	51
Figure 39. The Upper View of the DGS 1 : 8 BFN.	53
Figure 40. S-parameters for $d=0.5$, $w_d=2$, $l=2.5 : 0.5 : 3.5$ mm.	54

Figure 41.a. S_{11} for $l=2.5$, $d=0.5$, $w_d=1.4 : 0.2 : 1.8$ mm.....	54
Figure 42. S-parameters for the Defect Widths $w_d=1.8$, $w_{d2}=1.5$, $w_{d3}=1.3$, $w_{d4}=2.1$, $w_{d5}=2.3$ mm.....	55
Figure 43.a. S-parameters for the Resulting 1 : 8 BFN with 10 mm Distance between Ports ($l=2.5$, $d=0.5$, $w=1.15$, $w_d=1.8$, $w_{d2}=1.5$, $w_{d3}=1.3$, $w_{d4}=2.1$, $w_{d5}=2.3$).....	56
Figure 44.a. S-parameters for the Resulting 1 : 8 BFN with 21 mm Spacing ($0.7*\lambda_0$) Between Two Ports ($w=1.15$, $l=2.5$, $l_0=21$, $w_d=w_{d1}=1.8$, $w_{d2}=w_{d9}=1.5$, $w_{d3}=w_{d8}=1.3$, $w_{d2}=w_{d9}=2.1$, $w_{d3}=w_{d8}=2.3$ mm)..	57
Figure 45.a. Smith Chart Location for CuFlon RS-DGS Normalized to 50Ω , with $h=10$ mil, $w=0.8$, $w_d=1$ mm.	59
Figure 46.a. Smith Chart Location for Alumina RS-DGS Normalized to 50Ω , with $h=10$ mil, $w=0.27$, $w_d=0.5$ mm.	60
Figure 47.a. S_{11} for DGS T-junction Using CuFlon Substrate of $d=10$ mil, $w=0.8$, $w_d=1.2$, $d=0.05$, $l=0.75$, $d_p=2$ mm.	60
Figure 48. S_{11} for DGS 1 : 4 BFN with CST Using CuFlon Substrate of $d=10$ mil, $w=0.8$, $w_d=0.9:0.1:1.5$, $d=0.05$, $l=0.75$, $d_p=2$ mm with the Second Dielectric & Ground Added Beneath.	61
Figure 49.a. DGS 1 : 4 BFN with $w=0.8$, $w_d=1.2$, $l=0.75$, $d=0.05$, $l_0=6$, $d_p=1.25$ mm with the Second Dielectric & Ground Added Beneath.	62
Figure 50.a. S-parameters for the DGS 1 : 4 BFN with $w=0.8$, $w_d=1.2$, $l=0.75$, $d=0.05$, $l_0=6$, $d_p=1.25$, $w_{d2}=1.3$, $w_{d3}=1.1$ mm with the Second Dielectric & Ground Added Beneath.	64
Figure 51. S-parameters Phase Values for the DGS 1 : 4 BFN with $w=0.8$, $w_d=1.2$, $l=0.75$, $d=0.05$, $l_0=6$, $d_p=1.25$, $w_{d2}=1.32$, $w_{d3}=1.08$ mm with the Second Dielectric Added Beneath.....	65

Figure 52.a. Reflection Magnitude Characteristics of the DGS 1 : 4 BFN with $w=0.8$, $w_d=1.2$, $l=0.75$, $d=0.05$, $l_0=6$, $v_v=1.25$, $w_{d2}=1.3$, $w_{d3}=1.1$ mm with the Second Dielectric Added Beneath.....	66
Figure 53. Aperture-coupled Coupler Structure.	28
Figure 54. Aperture-coupled Structure with Perpendicular Placed Lines.....	29
Figure 55. S-parameters for the Aperture-coupled Power Divider.....	29
Figure 56. Aperture-coupled Divider with DGS Impedance Matching Circuitry.....	30
Figure 57.a. Power Loss vs. Freq. for No-Defect Case	31

CHAPTER 1

INTRODUCTION

With the enlarging application areas of the wireless technology, microwave engineers are forced to extend the in-use frequency band up to V and E bands from the first arising HF and VHF bands. As the frequency of interest has extended over the L band, standard lumped component approach has failed, and the implementation of the reactance was done by the short-line approximation which made use of the short-length transmission lines accomplishing the capacitive and inductive behaviors.

Short-line approximation is a modeling technique which was widely used as a standard method for the realization of the reactance in various filter applications. However, the design considerations of various filters have necessitated unrealizable transmission lines with non-standard line impedances, so new methods are widely encountered. Additionally, due to the variety of the design considerations, standard methods are overtaken by the novel, application-based methods.

Novel methods based on the design considerations of the designer are not only used in reactance realization or filtering applications, but used in any components of the microwave area by making use of the flexibility of the distributed elements.

Restrictions due to the realization of the transmission lines are encountered in any microwave components, even in the most basic ones. Considering the microstrip line, high impedance lines are implemented in the form of thin lines which requires a precise production technology.

In a systematic approach, i.e., if a system of microwave devices is considered, the non-standard line impedances have to be used frequently since they will be used for the impedance matching purposes and practically these non-standard impedance stubs are rea-

lized in the form $\lambda/4$ -length stubs. Hence, this standard approach makes the total structure bulky with the additional $\lambda/4$ -length stubs. Moreover, the non-standard line widths, and the transitions between the standard and the non-standard line widths are also distressed in terms of the production technology restrictions and radiation effects at the transitions.

If an application that can realize the non-standard impedances with standard line widths in shorter distances can be valid, then it would be convenient to use it in place of the standard impedance matching circuitries. This kind of a new application, of course, will have some advantages and disadvantages that also has to be considered before the implementation.

Defected Ground Structure (DGS) is the first application that comes to mind when the line is preferably not disturbed. A defect on the ground can change the propagation properties of a transmission line with changing the current distribution on the ground side, and the alignment of the fields between the ground and the line. Thus, novel microwave components like couplers, dividers, filters, impedance transformers can be made up. The structure in the most basic form consists of a line with defects on its ground (See Figure 1). The shape, dimension, repetition, etc. properties of the defect determines the utilization of the DGS.

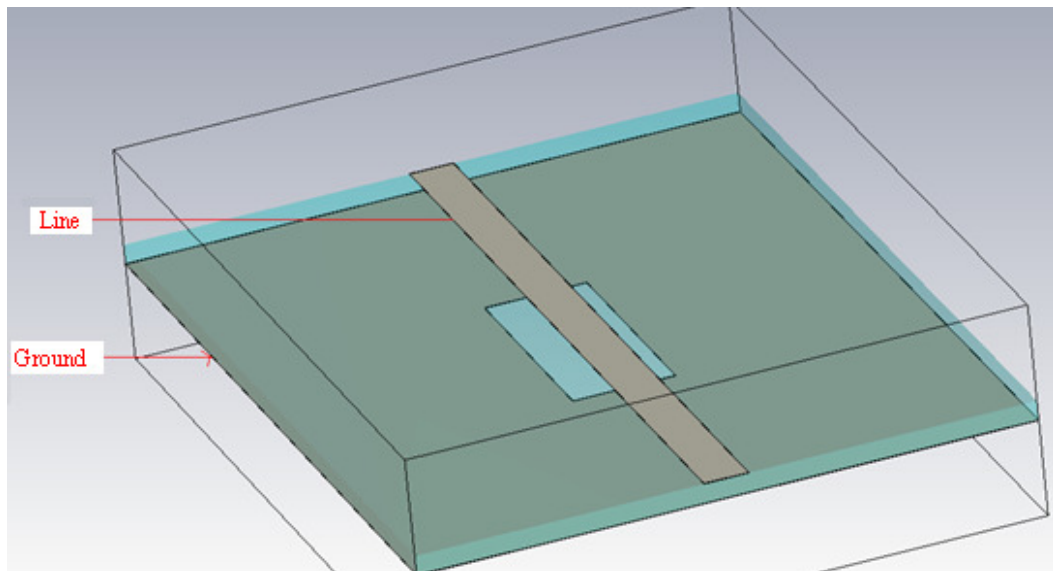


Figure 1. Defected Ground Structure for Microstrip Line.

The rectangular-shaped DGS (RS-DGS) resembles a transmission line structurally. Furthermore, it is observed to act as a high impedance transmission line [1-12]. Hence, RS-DGS can be used in the desired matching circuitries of the microwave components.

In this study, RS-DGS is used for its high impedance and slow-wave properties which make the designed microwave design compact and easy-to-implement. RS-DGS is implemented on the power divider and antenna feed network structures for matching, and power ratio variation purposes.

Organization of the thesis is as follows: Chapter 2 introduces a brief literature review of the defected ground structures (DGS). Furthermore, analysis on the rectangular-shaped defected ground structure (RS-DGS) is carried out for the characterization of the structure.

Chapter 3 focuses on the design of power divider design with RS-DGS at 10 GHz. Two types of power divider structures are covered; T-junction and aperture-coupled power dividers. T-junction is designed for the equal and unequal power division cases, and the aperture-coupled for unequal, and varying port power case. Additionally, the power loss examination of the aperture-coupled one is carried out.

In Chapter 4, the T-junction design by RS-DGS is extended to equi-phase, and equi-magnitude corporate antenna feed network at 10 GHz and 35 GHz. The 1 : 4, and 1 : 8 feed networks are designed at 10 GHz, and a 1 : 4 one is designed at 35 GHz. The implementation of the 10 GHz, 1 : 4 is also completed, and the corresponding measurements are presented.

Chapter 5 presents the conclusions of the thesis. The conclusions on the work completed, and the improvements achieved on each structure are expressed. Finally, the future work that can be performed on this subject is discussed.

CHAPTER 2

DGS ANALYSIS

There are various DGS studies in the literature not only for the analysis of the effect of the defects, but also for the implementation of the defects in various structures in microwave devices. It would be wise to have a look at the previous DGS studies first, and then present the contribution of this study.

2.1 Literature Review

The DGS studies conducted up to now have basically focused on the dumb-bell-shaped DGS which is basically proper for high frequency filtering applications [1-5]. The dumb-bell shaped defect is placed under the microstrip line as shown in Figure 2. Studies on the analysis of the structure have generally used the current density approaches [6] to model the structure. The current density distribution is determined not only by the line path, but also with the discontinuities on the ground; and the resulting current distribution is interpreted as a physical model [6]. After the physical modeling of the structure, the discontinuities are modeled in the form of the basic circuit components using the previous discontinuity studies [7-9]. These discontinuity studies, beyond their old age, are still valid, and efficiently used.

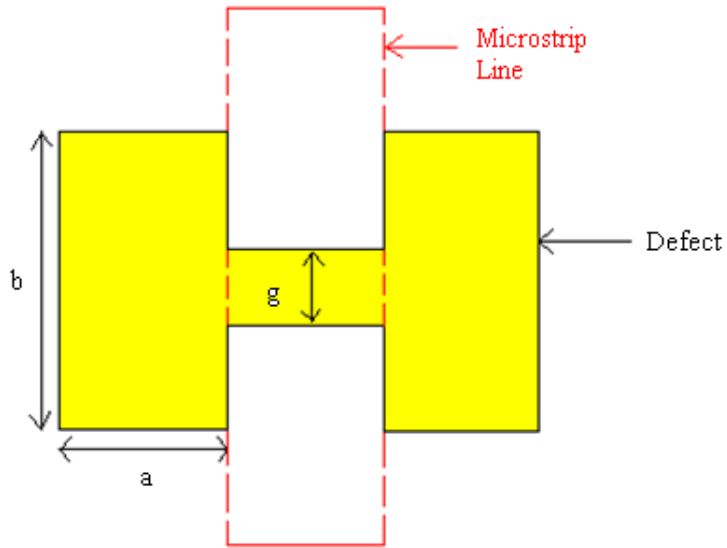


Figure 2. Dumb-bell Shaped DGS.

Another application of the DGS is the photonic band-gap structures (PBG). The promising effect of the band gap structures in microwave devices has generated the term electromagnetic band-gap (EBG) structure. These EBG structures are formed by the periodically distributed nonuniformities on the ground, substrate, or the line of a microwave component. These non-uniformities may be natural or synthetic. A periodically placed defect on the ground is a synthetic example of the kind [12].

In the literature, the dumb-bell shaped [1-5], periodically placed [12], L-shaped [9], and spiral-shaped [10] DGSs are investigated and implemented. The most basic form of all these structures is a rectangular shaped DGS, and this structure is implemented in this study.

The studies in the literature covered up to now are all of filter type or resonant type structures. However, non-resonant type applications of the DGS also exist. Rectangular-shaped defected ground structure (RS-DGS) resembles a transmission line due to its physical structure. In this aspect, it can be claimed that a RS-DGS can be modeled as a transmission line of characteristic impedance Z_{ch} not equal to the characteristic impedance of the line with the same line width. This might be helpful if we need to increase the impedance to the levels where line widths cannot be realized easily. The high characteristic impedance property of the DGS was first proposed by Kim [12], who emphasized

the high effective inductance of the DGS. This emphasis has taken the interest of the researchers who desire to implement high levels of impedance values which is impossible to realize using standard microstrip lines [13-19]. The N : 1 Wilkinson Power Divider was realized for N=4, and 6 by making use of 158 Ω and 207 Ω line impedances which was impossible to achieve with microstrip lines before the application of the DGS [17-19].

Impedance matching at shorter distances is also realized by the use of the slow-wave characteristics of the DGS in the case of the space saving applications like amplifier input-output matching circuitries, hybrid couplers [13-17]. The usage of DGS at the input or the output of the amplifiers has also confirmed harmonic-rejection, and efficiency improvement properties [14-17].

The effective-inductance improvement of DGS was also used to increase the even mode impedance, thus the coupling of an edge-coupled coupler with a rectangular-shaped DGS below the coupling lines [19]. This eliminated the necessity to decrease the distance between the coupled lines to unrealizable levels.

In this study, the rectangular-shaped DGS (RS-DGS) will be utilized for benefitting from its slow-wave and high impedance characteristics. The additional properties that may be uncovered and the adaptation of RS-DGS to newer forms will also be investigated.

2.2 The Rectangular-Shaped Defected Ground Structure (RS-DGS) Analysis

As stated before, in this study, DGS is applied to the ground of a microstrip line. The RO4003C substrate of Rogers Corporation at the 0.020 inch (0.508 mm) standard substrate thickness is chosen. The RO4003C substrate is utilized due to its low dielectric loss in the X-band frequencies.

The relative dielectric constant of the RO4003C substrate is specified as 3.38. The effective dielectric constant and the line width for the defined line impedance are necessarily calculated for the microstrip line. For this purpose, Microstrip Calculator is used, and the calculated results are verified by the simulation software employed.

The simulations of the designed structures are performed by CST MICROWAVE STUDIO®. CST MICROWAVE STUDIO® is outstanding due user friendly CAD tools, fast and reliable Transient Solver which allows you to observe the whole frequency domain

response of the system. For comparison purposes, ADS Momentum is also used in the design process.

By using the Microstrip Calculator, $50\ \Omega$ microstrip transmission line is found to have a width of 1.2 mm for the RO4003C 20 mil substrate which is optimized to 1.15 mm by the CST MICROWAVE STUDIO®. In the same way, $100\ \Omega$ microstrip transmission line width is found to be 0.29 mm, and optimized to 0.28 mm. With the help of the simulation results, effects of the defect on the ground are examined.

Figure 3.a shows the RS-DGS simulated as a microstrip transmission line with 1.15 mm line width and 2.65 mm defect width. Figure 3.b. shows a $100\ \Omega$ transmission line with 0.28 mm line width. The comparison of the two structures' Smith Chart results concludes to mark the same structure (See Figure 4 and Figure 5).

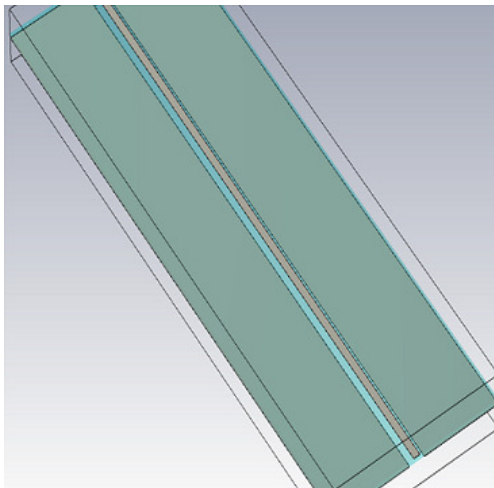


Figure 3.a. RS-DGS in the Form of a Transmission Line.

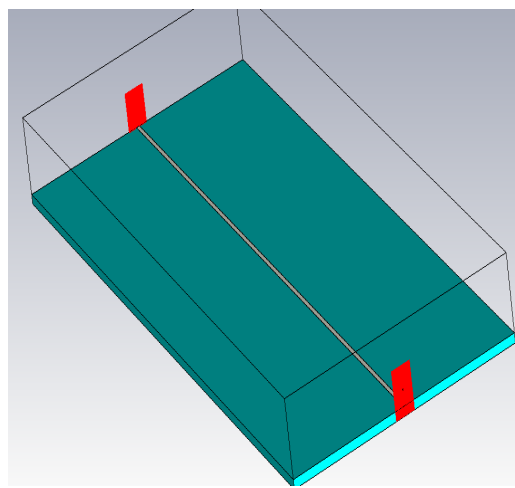


Figure 3.b. $100\ \Omega$ Transmission Line.

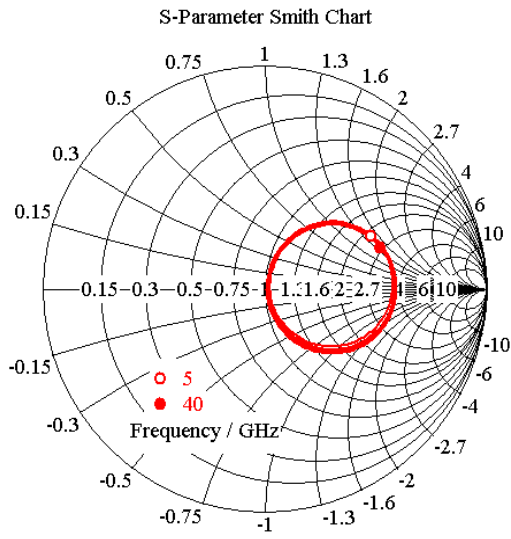


Figure 4.a. Smith Chart Location of the RS-DGS with 2.65 mm Defect Width Normalized to 50 Ω Port Impedance.

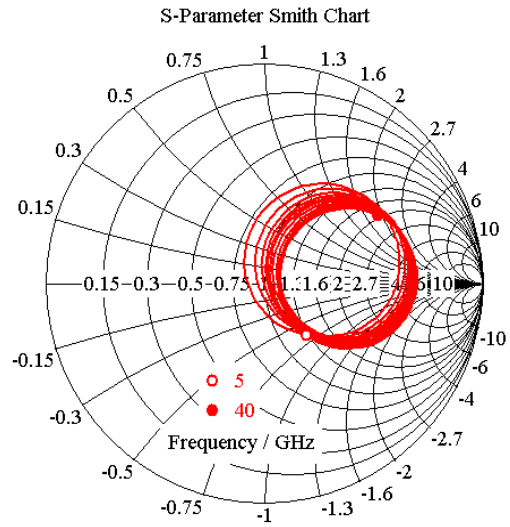


Figure 4.b. Smith Chart Location of a 100 Ω Transmission Line Normalized to 50 Ω Port Impedance.

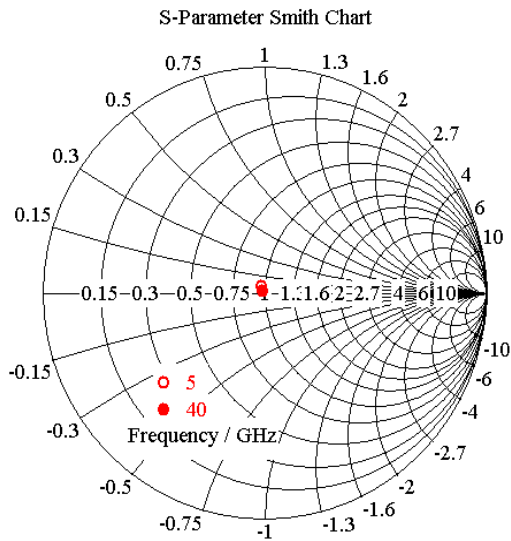


Figure 5.a. Smith Chart Location of the RS-DGS with 2.65 mm Defect Width Normalized to 100 Ω Port Impedance.

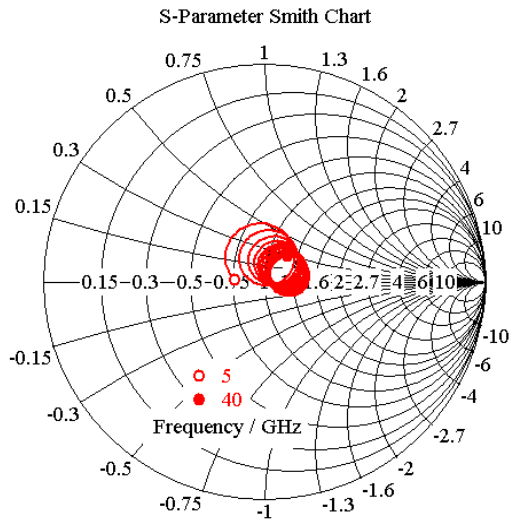


Figure 5.b. Smith Chart Location of a 100 Ω Transmission Line Normalized to 100 Ω Port Impedance.

The results for the RS-DGS transmission line show that from 5 GHz up to 40 GHz, the structure is perfectly matched to 100 Ω . The advantage of this structure can also be comprehended by checking the dimensions of the two structures. One can easily implement a 100 Ω line by using a RS-DGS structure with a 50 μm process technology. However, if classical 100 Ω line structure is used, one would need a process technology with better resolution accuracy.

The above results show the RS-DGS equivalence to 100 Ω impedance line. It can be claimed that the RS-DGS is equivalent to a high impedance line realized with a line width corresponding to 50 Ω line impedance. This result is not surprising since the previous studies state that the effective inductance of the defected ground structure is higher than that of a standard line [12]. Remembering the line impedance formulation of a low-loss line:

$$Z_{line} = \sqrt{\frac{L_l}{C_l}} \quad (1)$$

where L_l and C_l denotes the per unit length inductance and capacitance, respectively.

The placement of the defect on the ground increases the path of the ground currents, thus increases the inductance per unit length, L_l . Increase in L_l results in the increase of the line impedance. However, the effect of C_l also has to be considered. The capacitance can be claimed to be decreased since the distance between the ground and the signal line has increased. In the standard microstrip line, the fields are confined between the line and the ground, at the distance ruled by the thickness of the substrate, but when the defect is placed beneath the line, the fields confined between the ground and the line are inclined, resulting in an increased distance; hence a lower capacitance. The low capacitance is another factor increasing the line impedance. So, the effects of both L_l and C_l force the line impedance to increase.

The DGS line is proposed to have high line impedance, so the parameters that effect the line impedance can be investigated. There are two parameters that can affect the RS-DGS: the defect width with keeping the line width constant or the line width with defect width constant.

This study focuses on the effects of the defect, so changing the defect width is the chosen solution. Still, the effect of the change in the line width is observed. The simulated results expectedly show that the change in the defect width causes a change in the line impedance. The change can be considered as linear for frequencies above 5 GHz. The line impedance values versus defect width graph can be seen in Figure 6. The line impedance values are valid between 5 GHz and 40 GHz, that are the center values of all line impedance values for the corresponding defect width, and the maximum absolute deviation is 3 Ω .

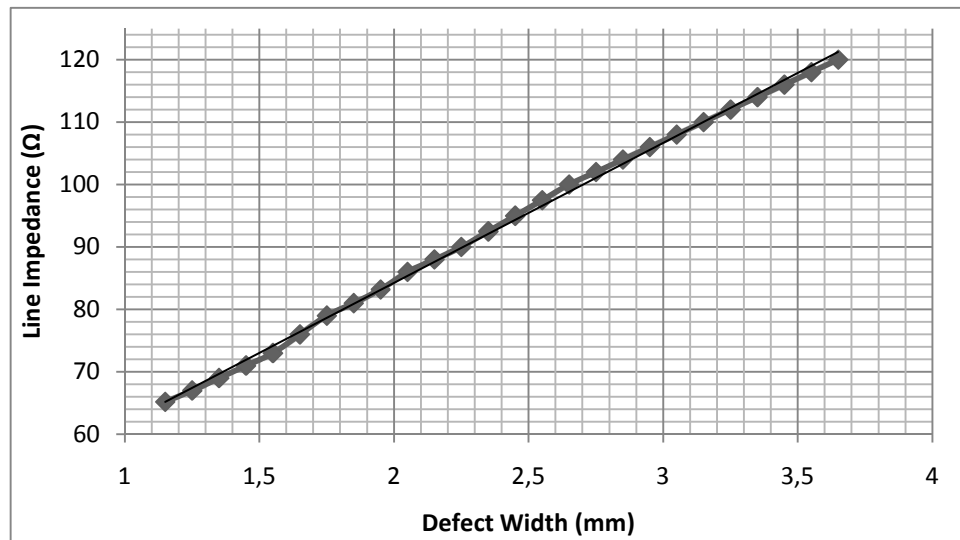


Figure 6. Line Impedance versus Defect Width.

It is obvious that there is a linear relationship between the line impedance and the defect width. This result is convenient to be used in the microwave devices. However, for the sake of completeness, the change in the line width is examined by keeping the defect width constant. The defect width is kept as 2.65 mm which corresponds to 100 Ω line impedance with the regular 1.15 mm line width. The line impedance for varying line width (Defect width=2.65 mm) can be seen in Figure 7. The impedance values are still valid above 5 GHz and are the center values of the all frequencies between 5 GHz and 40 GHz, the maximum absolute deviation is 3 Ω .

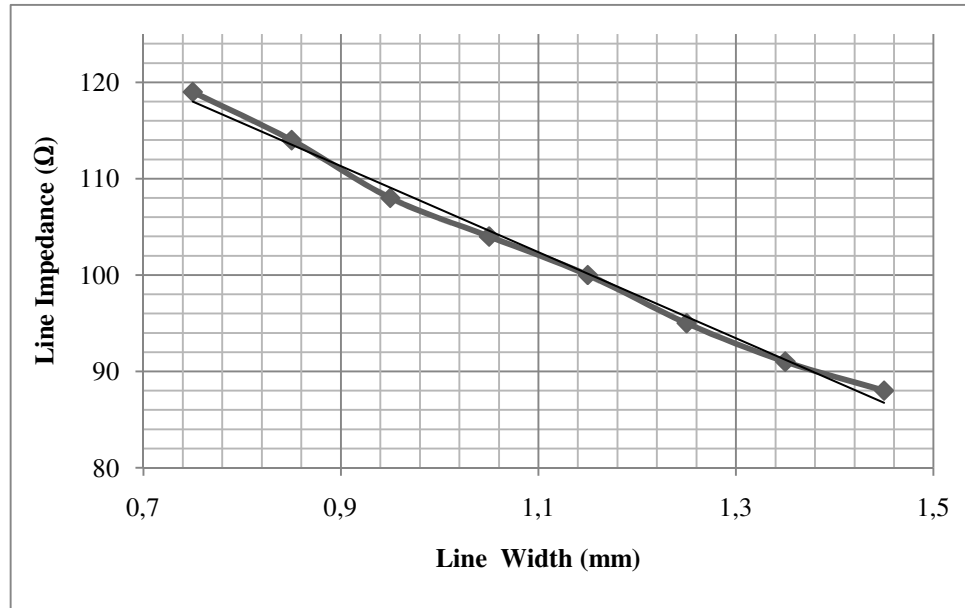


Figure 7. Line Impedance versus Line Width.

In Figure 7 it is observed that the line width also changes the line impedance. In fact, this result is not surprising since the impedance is directly linked to the line width for the microstrip lines. However, considering the insertion of the RS-DGS into a 50Ω system, the preference would be to use the same width. For example, designing a beam forming network, the necessity for the varying width lines diminish by the use of the defects. The advantages and the disadvantages of the DGS are further discussed in the application parts.

In the most basic form, the application of a RS-DGS can be the insertion of a piece of the structure into a system. At this step, the question that comes to mind is the wavelength of the structure. If the modeling of the RS-DGS as a high impedance line is considered, the length can be considered as the length of the non-standard ($\neq Z_{ch}$) impedance line. However, at this point wavelength comes to the mind. Would the wavelength of a RS-DGS be the same as the corresponding high impedance line? Figure 8 shows the S_{11} & S_{21} figures of the RS-DGS corresponding to 100Ω impedance, and the 100Ω line impedance.

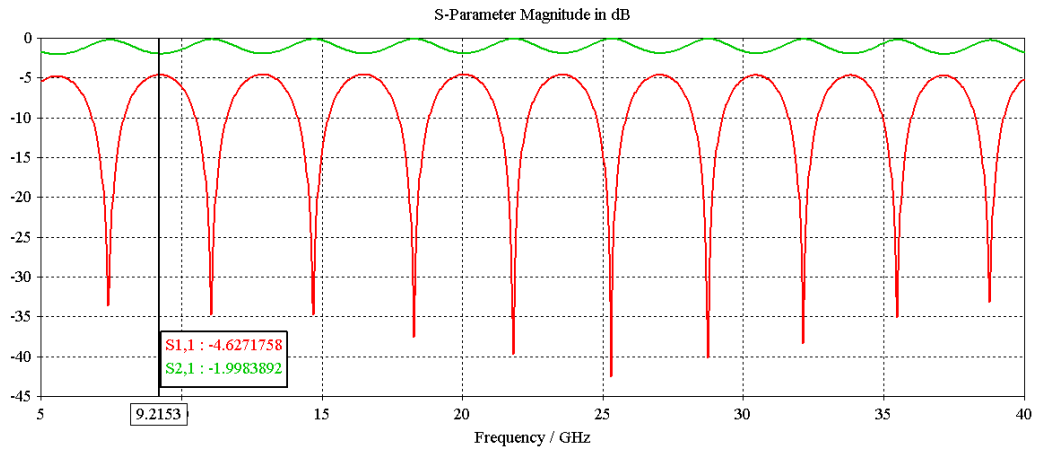


Figure 8.a. S-parameters of the 100 Ω-Line-Impedance RS-DGS with 50 Ω Port Impedance.

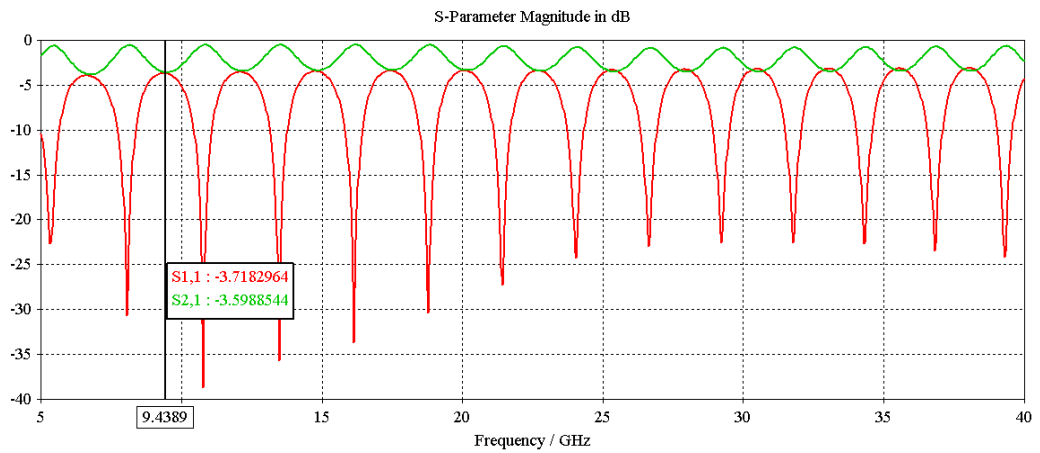


Figure 8.b. S-parameters of the 100 Ω-Line-Impedance Microstrip Line with 50 Ω Port Impedance.

It is observed in Figure 8 that the wavelengths of the two structures do not fit. Hence, it can be concluded that DGS shows slow-wave characteristics. At this step, it would be wise to check the per unit length inductance and capacitance values, L_l and C_l , since they are directly related to the phase velocity with the formula:

$$v_p = \frac{1}{\sqrt{L_l C_l}} \quad (2)$$

It was proposed that L_l increases, and C_l decreases for a DGS line, and the slow-wave characteristics show that the product of the two decreases. Then, it can be concluded that the increase in L_l is more dominant than the decrease in C_l .

However, the direct formulation of the wavelength will not be carried out in this study. The defect parameters will be optimized for the desired operation frequency. In order to investigate the change in the length of the defect, the network in Figure 9 is formed.

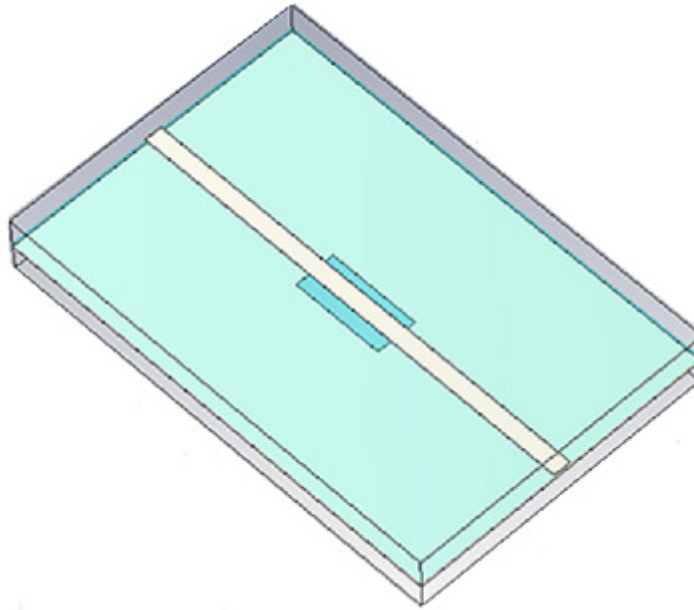


Figure 9. RS-DGS with Varying Length Defect.

The S_{11} & S_{21} results of the RS-DGS for three different defect length values can be seen in Figure 10. The simulated defect lengths are 3 mm, 6 mm, 9 mm. Defect width is 2.65 mm since 100 Ω lines are desired to be imitated. The structure with 100 Ω lines instead of the defect is also simulated and shows nearly the same results with the RS-DGS, but for the sake of simplicity, those results are not demonstrated here.

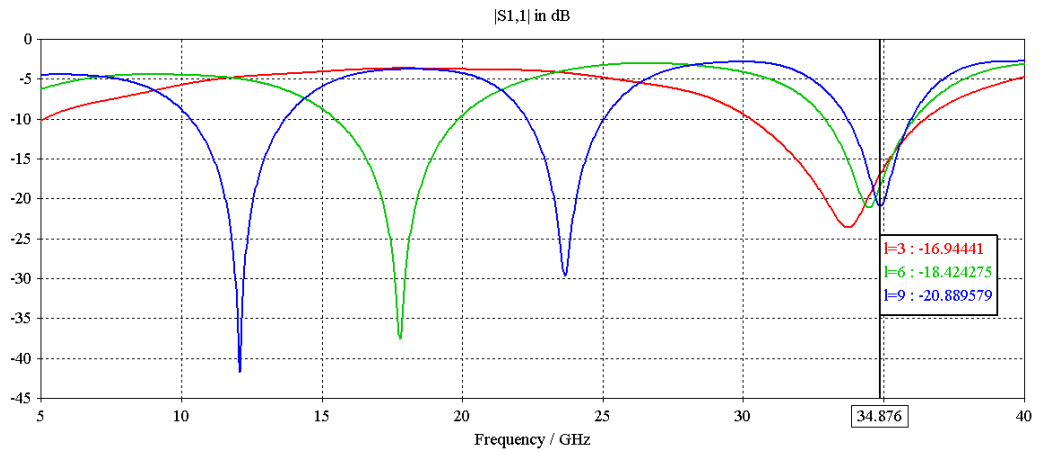


Figure 10.a. S_{11} for the RS-DGS with $w_d=2.65$, $l=3, 6, 9$ mm.

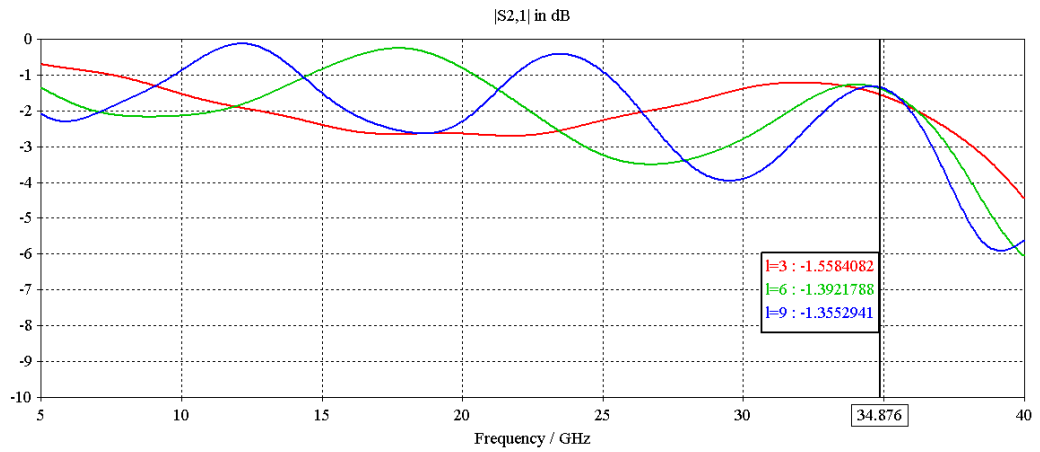


Figure 10.b. S_{21} for the RS-DGS with $w_d=2.65$, $l=3, 6, 9$ mm.

The length of the defect changes the resonant frequency. Considering the RS-DGS as a resonant structure, a possible conclusion may be the length of the defect is directly proportional to the resonant frequency. Others may be the periphery, or the area of the defect, even the width of the defect is directly proportional to the resonant frequency. However, due to the lack of tightness of the current density in the defect width direction, the effect of defect width is not directly felt at the resonant frequency [6]. Resonant frequency is mainly controlled by the defect length, and the defect width also has some impact on it [6]. This can be checked by the results in Figure 10.

Referring to Figure 10, resonant frequency at 3 mm defect length is 34.8 GHz, if the defect length was the only factor to control resonant frequency; it would be halved when the defect length increases to 6 mm. However, the resonant frequency falls to 17.8 GHz instead of 17.4 GHz, and falls to 12.1 GHz instead of 11.6 for 9 mm defect length. These deviations can be considered as the effect of the width. The effects of the defect width at the resonant frequency for different defect lengths can be investigated. However, it would be time wasting in this study. Besides, the defect length can be used directly to detect the resonant frequency since the shift due to the defect width is small, and can be ignored.

Once investigating the whole parameters of the DGS, the usage of the structure in the microwave devices for various applications can be summarized. These applications are basically impedance matching networks used in the T-junctions, beam forming networks, and couplers.

CHAPTER 3

POWER DIVIDER

Applications of RS-DGS may be present in any microwave system because it can be used in impedance matching networks that are essential in most of the microwave circuits. This study examines the application on some specific devices, and focuses on the novel applications which were not covered before in literature. The ultimate aim of this chapter is application of RS DGS in a beam forming network.

3.1 T-junction

T-junction is frequently used in microwave systems as in the building block of a feed network, and the main power division element of the large scale microwave networks. Implementation of the RS-DGS on the T-junction has great advantages in terms of simplifying the production process. However, the alignment of the defect with the line may be a problem which can be easily solved with a careful work.

3.1.1 Equal Division T-Junction

Equal power division is incorporated in the junction design. Thus T-junction is realized as seen in Figure 11 in the most basic form. The standard 50Ω line has to be connected to two parallel 100Ω impedances, so the matching is guaranteed. For this purpose, the 50Ω lines which also terminate the output of the system are converted to 100Ω with $\lambda/4$ (70.7Ω) impedance matching networks. The 70.7Ω lines are the thin lines in Figure 11, where the thick lines are 50Ω lines.

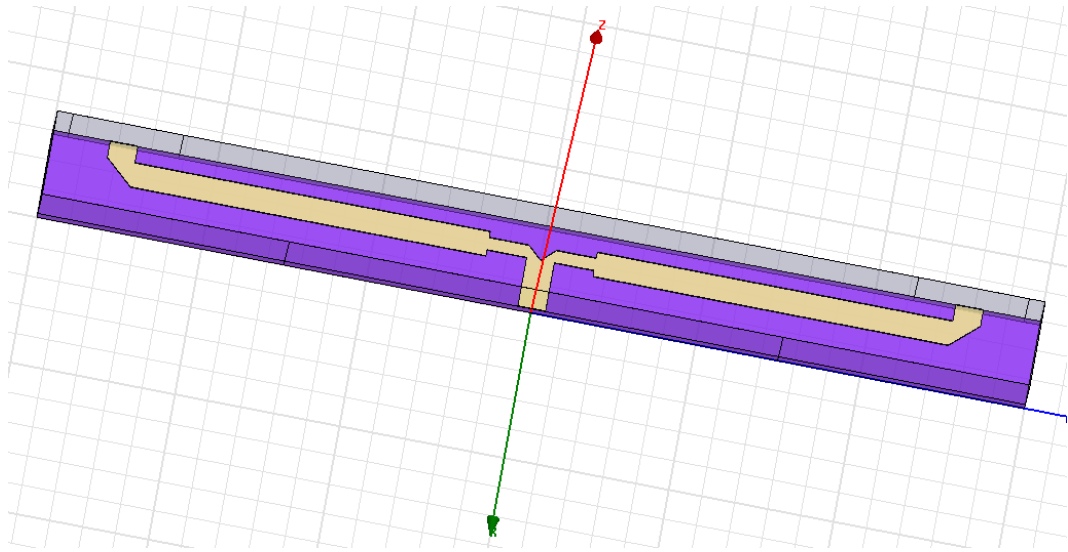


Figure 11. Standard Microstrip T-junction.

The purpose of using RS-DGS structure is to improve the standard T-junction structure in its design and performance. The advantage of the RS-DGS is the removal of the discontinuity or step effects in the line. However, the radiation from the defect on the ground is a disadvantage for the RS-DGS. These two effects may compensate each other, but the advantage of the RS-DGS is the removal of the necessity of fine process. There is no need to process the recesses or protrusions. The general structure of a T-junction with RS-DGS matching sections can be seen in Figure 12.

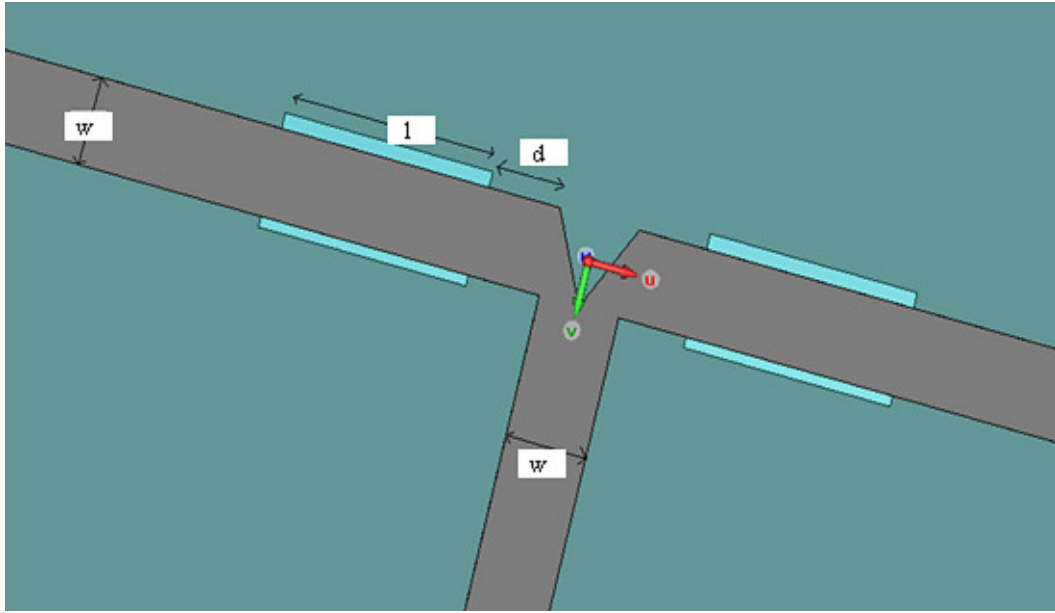


Figure 12. T-junction with RS-DGS Matching Section.

In the standard structure, the distance between the high impedance line and the junction is zero ($d=0$), and the non-standard line is a 70.7Ω , $\lambda/4$ line transforming 50Ω to 100Ω . The same structure can be implemented with RS-DGS by using a rectangular defect of 1.45 mm width.

There does not exist a commonly used formula for the calculation of the wavelength of the structure, but the wavelength at the desired frequency can be found by sweeping the defect length, and checking the resulting S-parameters.

The results of the defect length sweep can also be used as a parameter for a resonant frequency versus defect length table. However, this would not be helpful, further it would be time-wasting. The simulation result of the T-junction with $d=0$ mm and defect width=1.45 mm is expected to be matched at the desired frequency after setting the defect width (w_d). The corresponding result can be seen in Figure 13.

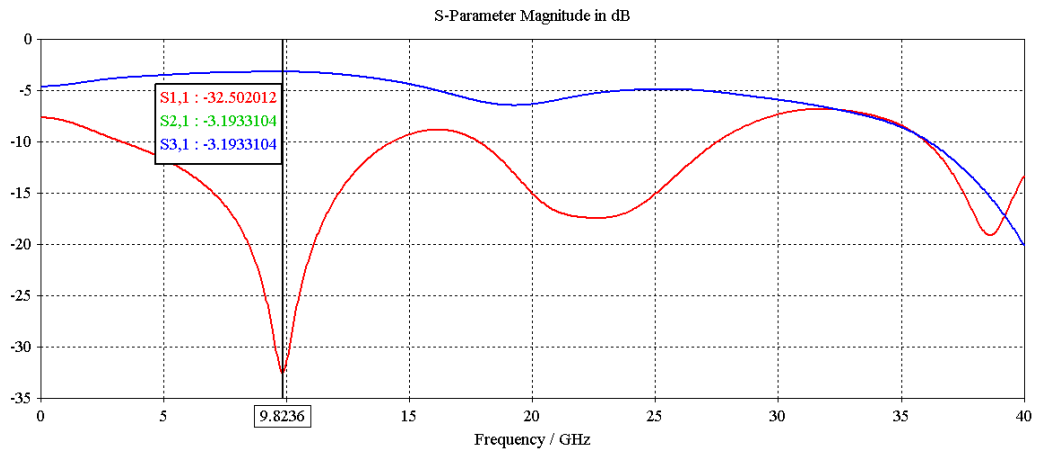


Figure 13. Results for the RS-DGS T-junction with $d=0$, $l=4.4$, $w_d=1.45$ mm.

S-parameters show that an acceptable matching level in the X-band can be obtained. Another parameter to make the structure more compact may be the distance from the junction, d . The distance from the junction (d) and the defect length (l) are also related with the resonant frequency. So the optimum d , l combination that makes the total length smallest for the X-band can be found. The effect of the defect width (w_d) is to find the best match impedance at the desired frequency. So, the design procedure starts with finding the d , l pair, and then finding the w_d that best fits to the d , l pair.

In order to find the optimum d - l pair, d - f_0 & l - f_0 relation must also be analysed. S_{11} versus frequency for various d values is given in Figure 14 which shows us the dependence of f_0 on d for $d=0.2, 0.3, 0.4, 0.5$ mm. At every d value, defect width (w_d) takes the values that guarantee a good matching level.

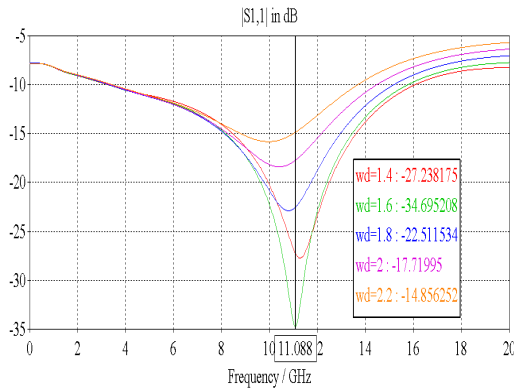


Figure 14.a. S_{11} for $l=3$, $d=0.2$, $w_d=1.4:0.2:2.2$ mm.

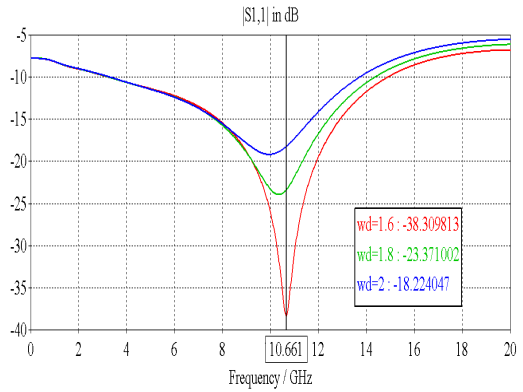


Figure 14.b. S_{11} for $l=3$, $d=0.3$, $w_d=1.6:0.2:2.0$ mm.

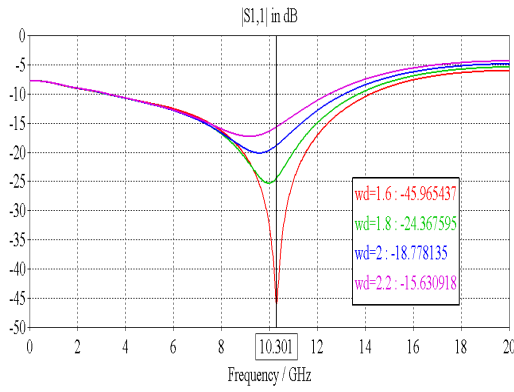


Figure 14.c. S_{11} for $l=3$, $d=0.4$, $w_d=1.6:0.2:2.2$ mm.

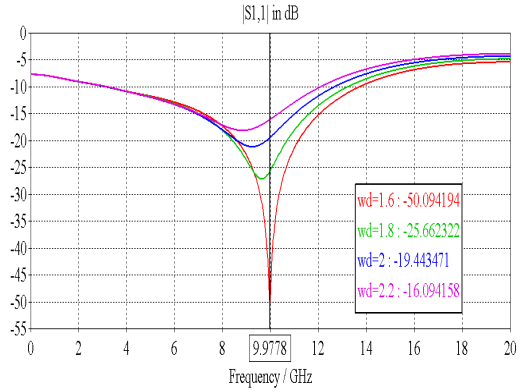


Figure 14.d. S_{11} for $l=3$, $d=0.5$, $w_d=1.6:0.2:2.2$ mm.

Note that as the distance from the junction increases, the resonant frequency decreases which is the nominal case in the standard T-junctions also. As the frequency decreases, the physical dimensions start to increase, i.e. the transforming sections start to take more places in the regular $\lambda/4$ transformers. The aim in the RS-DGS impedance transformer is to make the most compact design. So, the d - l pair that will conclude in the shortest length at the highest frequency is desired to be obtained. For this purpose, S_{11} versus defect width (w_d) graph for various l values is given in Figure 15 which shows us the dependence of f_o on l for $l=2, 3, 4$ mm.

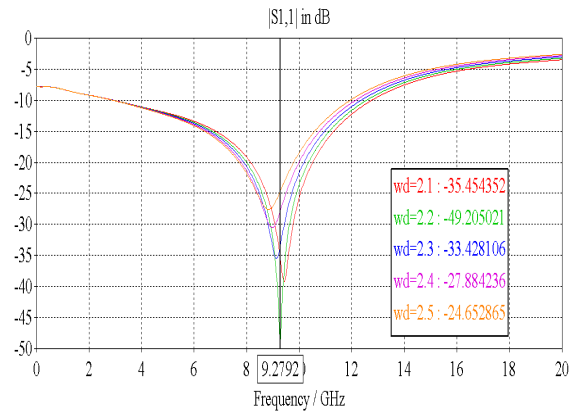


Figure 15.a. S_{11} for $l=2$, $d=1$, $w_d=2.1:0.1:2.5$ mm.

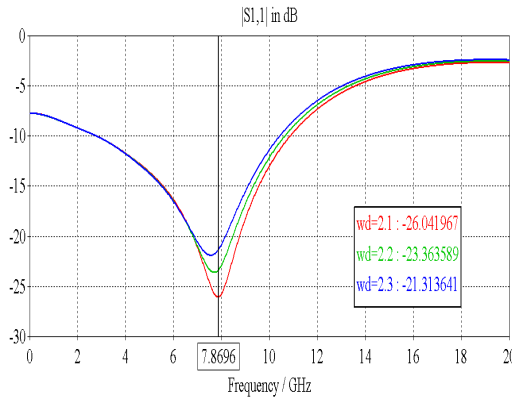


Figure 15.b. S_{11} for $l=3$, $d=1$, $w_d=2.1:0.1:2.3$ mm.

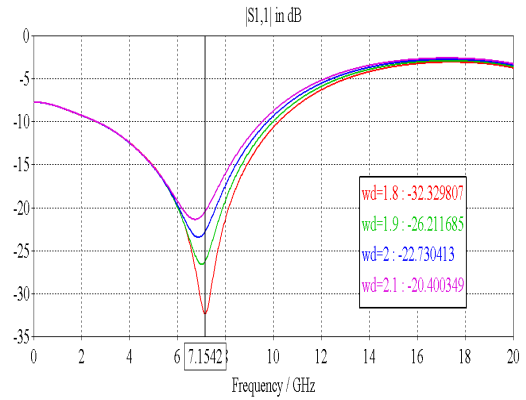


Figure 15.c. S_{11} for $l=4$, $d=1$, $w_d=1.8:0.1:2.1$ mm.

Comparing Figure 14 & Figure 15, one can conclude that approximately 0.1 mm change in d results in about a 0.3 GHz resonant frequency change, and 1 mm change in l results in the resonant frequency change of 0.7 to 1.4 GHz. At this point, it would be wise not to consider the complete frequency domain, but to consider the frequency region of interest. The selection of d which results in the resonance at the lower X-band would result in a shorter l , with only a small increase in d . The selection of d as 0.5 mm, which gives a resonant frequency at 9.97 GHz with $l=3$ mm would be the optimum choice.

The RS-DGS transformer is claimed to be more compact now, but the comparison of the RS-DGS with the regular $\lambda/4$ transformer would show us the results. Notice that $d = 0.5\text{mm}$ & $l = 3\text{ mm}$ combination brings resonance at 9.97 GHz; the frequency at which $\lambda/4$ corresponds to 4.6 mm, which shows that the device designed by the new RS-DGS would occupy 24 % less place. In the same way $d=0.4\text{ mm}$ & $l=3\text{ mm}$ combination brings resonance at 10.3 GHz, at which $\lambda/4$ corresponds to 4.7 mm (23.6 % less place). The comparison of these two results also support that as d decreases, it yields a sharper increase in resonant frequency that would be difficult to compensate with a suitable defect length.

The chosen d - l values ($d=0.5\text{ mm}$, $l=3\text{ mm}$) give resonance at 9.97 GHz. In order to reach resonance at the desired frequency, simulations are carried on for varying defect lengths when the distance from the miter is kept 0.5 mm. The corresponding results can be seen in Figure 16.

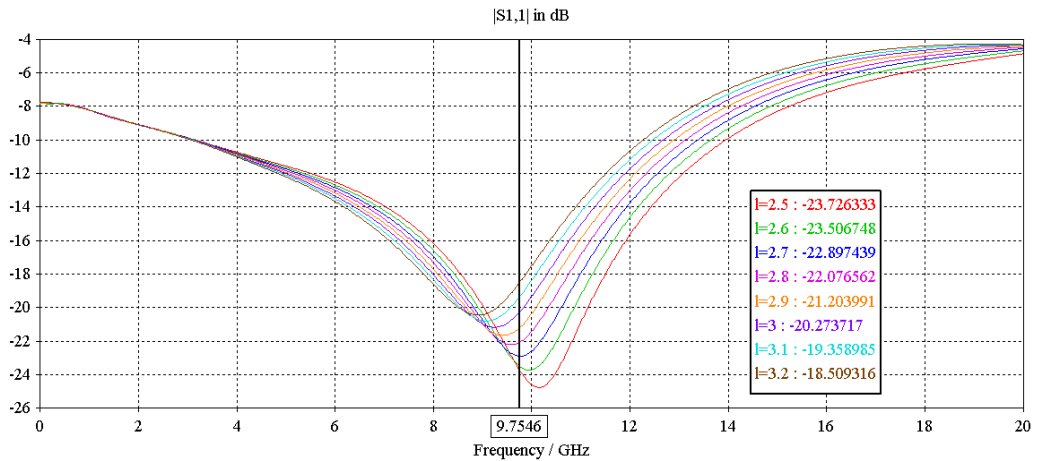


Figure 16. S_{11} for $l=2.5 : 0.1 : 3.2$, $d=0.5$, $w_d=2\text{ mm}$.

If the desired frequency is chosen as 9.75 GHz which can be considered as the center of the X-band, 2.7 mm is the best fitting condition for $d=0.5\text{ mm}$, and $w_d=2\text{ mm}$ at 9.75 GHz. The total length, to compare with $\lambda/4$ is 3.2 mm which is 1.51 (4.71-3.2) less. The total length is 32 % shortened for the desired resonant frequency 9.75 GHz. If the S_{11} level at the resonance was higher than the acceptable value, the defect width (w_d) would be varied, and the optimum value of that would be found.

3.1.2 Unequal Division T-Junction

The basics of the T-junction using RS-DGS is summarized in the equal division T-junction section. The unequal division T-junction realization is also done by unequal width $\lambda/4$ lines in the standard structures. However, as the division ratio increases, one of the line impedances start to rise sharply, which is impossible to implement with the standard thin lines.

While implementing an $N : 1$ divider, the division ratio N regulates the impedances of both sides. This would be realized directly by the previously found line impedance values if the distance from the junction to defect (d) was chosen as zero. However, with a nonzero distance, the selected RS-DGS will transform 50Ω to a different impedance, and that impedance is transformed through the 'd' length also. Considering both these effects is a long and a time wasting activity. Instead, the iteration method using the variable sweep option of the CST Simulation Software can be used.

Since the division is unequal, the impedance difference between the two lines seen from the junction must be maximum. For this purpose, defect width at one of the sides is chosen as 1.15 mm which is equal to the line width of the 50Ω line. It is also convenient to remember that $d=0.5$, $l=2.7$ mm is still valid. The effect of the defect width lower than the line width is also simulated, and the result is decreasing line impedance converging to 50Ω . Another factor that has to be taken into account is the equivalent impedance of the two ports. The equivalent impedance must be equal to the input port impedance 50Ω . This will also be checked during the iteration process. If the matching is not guaranteed, the S_{11} value at the resonant frequency is high. The defect width at the Port 3 side, w_{d3} is chosen as 1.15 mm and the defect width at the Port 2 side, w_{d2} is varied between 2.45 mm and 3.25 mm. The corresponding results can be seen in Figure 17.

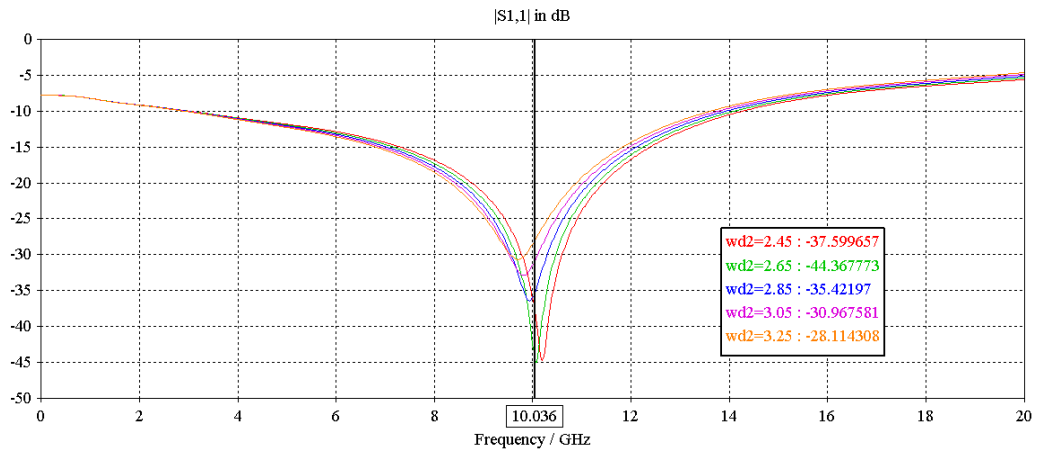


Figure 17.a. S_{11} for $l=2.7$, $d=0.5$, $w_{d2}=2.45 : 0.2 : 3.25$ mm.

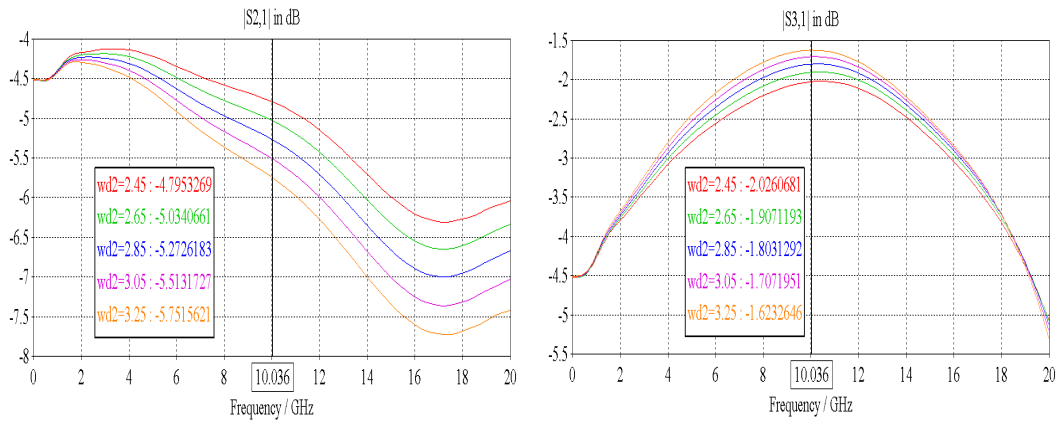


Figure 17.b. S_{21} for $l=2.7$, $d=0.5$, $w_{d2}=2.45 : 0.2 : 3.25$ mm. Figure 17.c. S_{31} for $l=2.7$, $d=0.5$, $w_{d2}=2.45 : 0.2 : 3.25$ mm.

The resonant frequency changes from 9.72 GHz to 10.19 GHz with the varying width. The resonant frequencies have increased compared with the equal division case since the widths have also increased. However, the 20 dB band of S_{11} does not significantly change. The power ratios between the ports also change with varying width. Illustration of both the resonance frequency, power division ratio, and 20 dB S_{11} band with respect to defect width at Port 3 when the defect width at Port 2 is 1.15 mm is provided in Table 1. The data are taken from Figure 17.

Table 1. Defect Width Effect to Unequal Division for the Constant 1.15 mm Defect Width at the 2nd Port.

Defect Width (mm)	Power Division Ratio	Resonance Frequency (GHz)	20 dB Band (%)
2.45	1.9	10.19	26.2
2.65	2.05	10.07	26.7
2.85	2.2	9.93	26.9
3.05	2.38	9.82	26.8
3.25	2.55	9.72	26.7

3.1.3 Addition of Second Dielectric under the DGS Layer

The most apparent problem that may be encountered while using a DGS in a feed system is the radiation emitted from the defect. The addition of a dielectric layer under the DGS may be a solution to this problem which would also be helpful if the T-junction is desired to be placed in a metal box. If no dielectric is added under the DGS, the structure cannot be put into a metal box since the metal box will fill the defect and the defect is shorted out. Even if the T-junction is placed in a non-metal box, the effects of the box dielectric on the structure performance have to be tested. A test period of two stages is necessary at this step; the simulation of the structure with a second dielectric of different lengths and a radiation boundary underneath, and the same simulation with a metal boundary underneath.

The test period of the structure with the added dielectric underneath has shown us that if the dielectric is thick enough, it has no effect on the performance of the structure. Simulation results show that the threshold thickness can be considered as five times the substrate thickness ($5 \times h$). However, as the thickness of the lower dielectric is decreased beneath $5 \times h$, the frequency of operation, i.e. resonance frequency starts to shift. This shift in the frequency is balanced with a change in the defect length that would set the resonance frequency to the desired value.

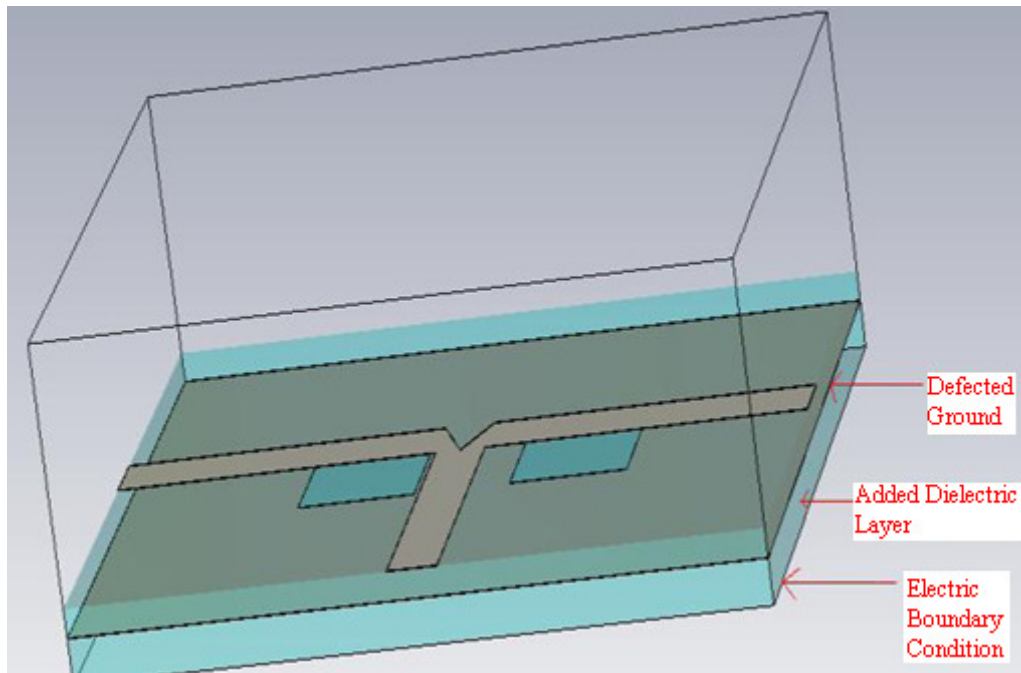


Figure 18. Schematic View of a Dielectric-Added DGS.

The realistic model with a dielectric of standard thickness 32 mil, 0.8128 mm can be seen in Figure 18.

Remembering the T-junction design at with 2.7 mm defect length (l), 2 mm defect width (w_d), and 0.5 mm distance between junction and defect (d); (See Figure 16) the resonant frequency was noted as 9.75 GHz. The dielectric-added structure is also simulated for the same design variables l , w_d , and d . The corresponding S-parameters can be seen in Figure 19.

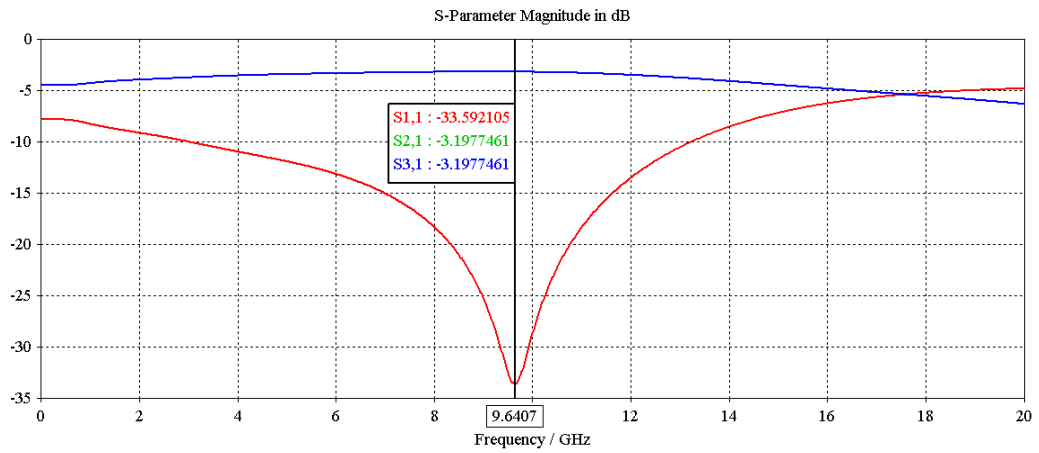


Figure 19. S-parameters for the Dielectric-Added DGS with Parameters $l=2.7$, $d=0.5$, $w_d=2$ mm.

The only change is the resonant frequency after the addition of the dielectric. The design considerations staying unchanged, with only variation in l , the resonance frequency can be shifted to 9.75 GHz. The addition of the second ground beneath the second dielectric does not make a significant change in the resulting S-parameters. Consequently, the addition of the dielectric and another ground below the defected ground makes a predictable change in the design.

3.2 Aperture-Coupled Unequal Power Divider

Utilization of an aperture in a layered structure is widespread in the design of couplers. The standard coupling parameters of the edge-coupled coupler are replaced with the coupling parameters of the new structure which are aperture area, and line coupling area. The analysis is carried out for these parameters, and their relation with the coupling coefficient is clarified [29-31]. The results are satisfying, and are used in various designs [31-33]. Figure 20 shows the general shape of the aperture-coupled coupler structure with a rectangular-shaped aperture.

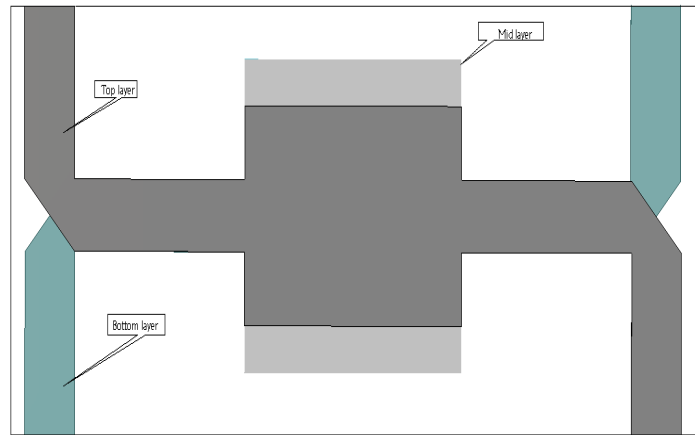


Figure 20. Aperture-coupled Coupler Structure.

In the above mentioned structure, two parallel lines are coupled via an aperture. The resulting structure is a four-port device with one of the ports isolated. So, the resulting device can be considered as a three-port device. In the context of this study, the two lines that are coupled through an aperture are placed perpendicular, and are still coupled via an aperture. The proposed structure cannot be modeled as a coupled line since the isolated and coupled port definitions are not valid for this structure. On the other hand, it can be classified as a multi-layer, aperture-coupled power divider. The proposed structure can be seen in Figure 21.

The coupling area can be quadratic or circular in the perpendicular-placed lines. However, in order to reduce the radiation from the edges of a square, the circular aperture is preferred.

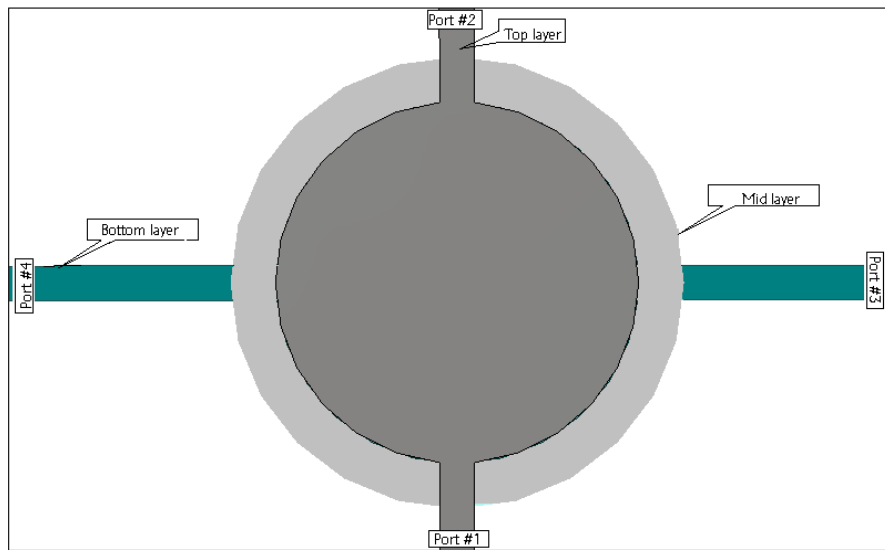


Figure 21. Aperture-coupled Structure with Perpendicular Placed Lines.

20 mil Rogers R4003C substrate is used in the design procedure, and the structure parameters are optimized for operation at 10 GHz. These parameters are line coupling radius, and aperture radius.

As can be seen in Figure 22, the coupled power is equally shared by the two coupled ports; Port #3, and Port #4; and none of these ports is isolated.

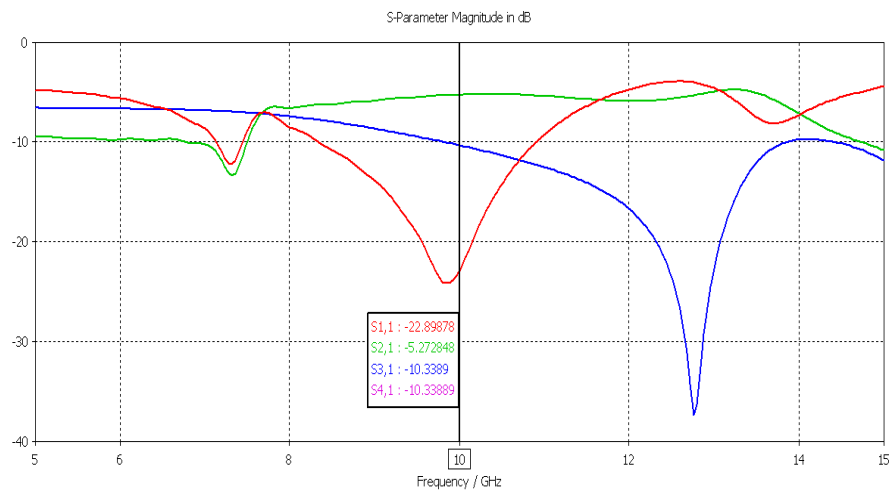


Figure 22. S-parameters for the Aperture-coupled Power Divider.

The S_{i1} ($i=1:4$) at 10 GHz are as follows:

$$S_{11} = -23\text{dB} \quad S_{21} = -5.27 \text{ dB} \quad S_{31} = S_{41} = -10.4 \text{ dB}$$

The equalization of the ports 3 & 4 can be terminated by adding impedance transformers to one of the ports which necessarily should not create a mismatch at the reflection of the feed port, i.e., S_{11} should be kept under control. The impedance transformation is done by the utilization of defected ground structure (DGS) which can be used in the impedance matching circuits [33-34]. The divider structure with the defect added in the mid layer (ground), below the feed line of the Port #3 can be seen in Figure 23.

The addition of the DGS led to the addition of new parameters. These parameters are the defect length (l_3), and the distance of the defect from the aperture (d_3).

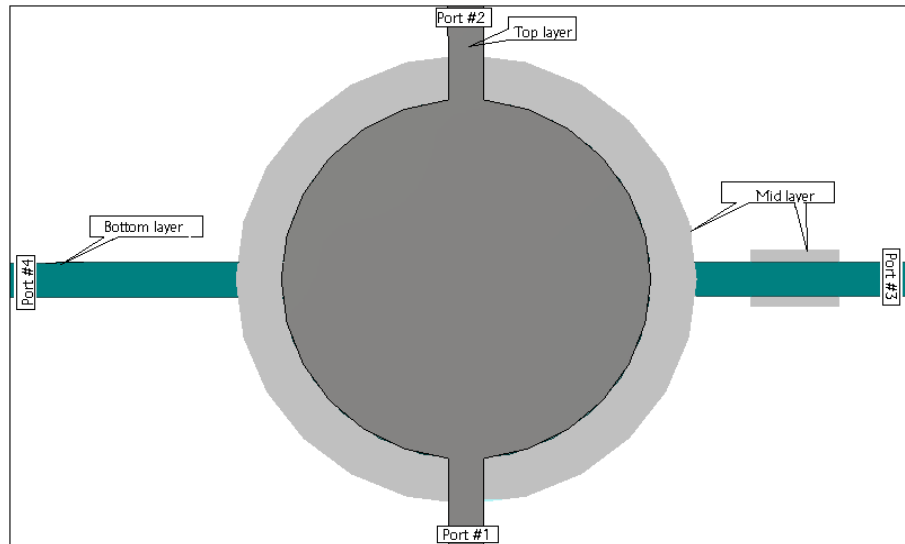


Figure 23. Aperture-coupled Divider with DGS Impedance Matching Circuitry.

The power division can be arranged in order to provide the desired ratio between the ports with keeping the return loss at acceptable levels. However, one disadvantage is the power efficiency of the device.

As clearly seen from Table 2, power distributed to the 2nd, 3rd, and the 4th ports is below the ideal level, and the insertion loss of the structure is at high levels. The DGS has also effects on the power loss means of the structure. This can be easily checked by comparing the two data; no defect, and defect at the 3rd port data. Thus, the power loss examination of the structure would also be beneficial in the context of this study.

Table 2. Power Division Ratios.

l3 (mm)	d3 (mm)	S ₁₁ (dB)	S ₂₁ (dB)	S ₃₁ (dB)	S ₄₁ (dB)
0	0	-23	-5.27	-10.4	-10.4
2	2	-30.1	-5.6	-10.5	-9
3	3	-28	-5.66	-11	-9.3
4	4	-23	-5.2	-11.4	-11

3.2.1 Power Efficiency Examination

The efficiency of the structure is tested, and the corresponding loss calculations are carried out in the 1 GHz – 20 GHz band. The task is performed for the two cases; no defect, and 4-mm-defect cases, which also allows the notification of the defect related loss. The corresponding results can be seen in Figure 24.

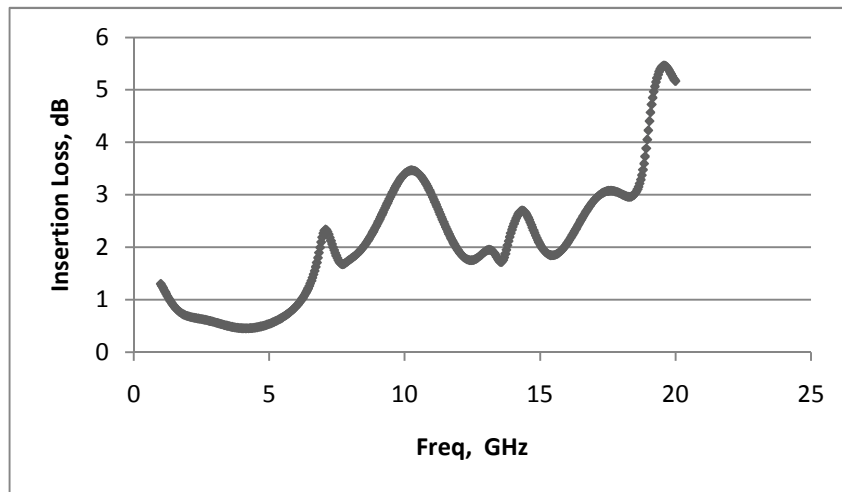


Figure 24.a. Power Loss vs. Freq. for No-Defect Case .

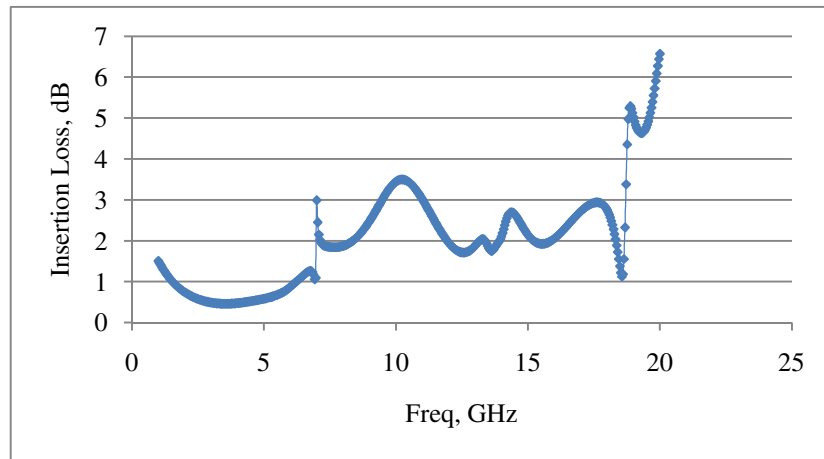


Figure 24.b. Power Loss vs. Freq. for 4-mm-Defect Case.

The loss mechanism has two main components, dielectric losses and radiation losses. Referring to the previous studies [31-33], and the properties of Rogers R4003C substrate, it can be claimed that the dielectric losses are not of importance at these frequencies. The only difference that makes this structure novel is the novel orientation of the lines, and the aperture. So, it would be convenient to state that the main source of the loss in this device is the radiation from the aperture, and the defect.

CHAPTER 4

BEAM FORMING NETWORK

The standard beam forming network (BFN) in the microstrip line technology are realized by using thin and thick lines which are utilized for the realization of the high and low impedance lines. The standard view of a basic 1 : 8 BFN can be seen in Figure 25. The standard 1 : 4 and 1 : 8 BFN structures is realized by using RS-DGS.

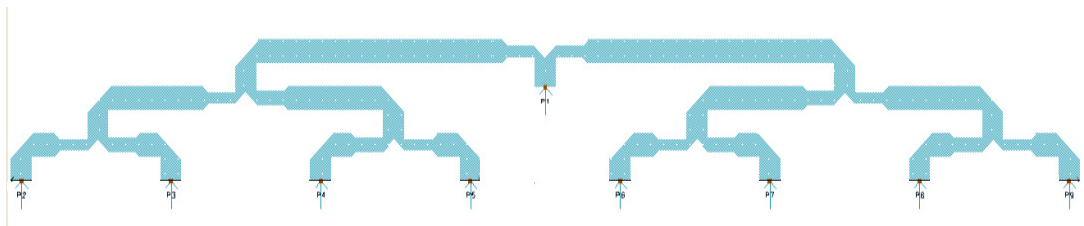


Figure 25. Standard 1 : 8 BFN.

4.1 DGS 1 : 4 BFN Design

The proposed DGS T-junction was claimed to be the first step of a BFN. So, a 1 : 4 structure is also designed with RS-DGS instead of standard impedance transforming lines. The resulting structure is also expected to be resonant at 10 GHz, the resonance frequency of the 1 : 2 structure. However, the resultant characteristics do not show resonance at 10 GHz. The change in the line length may be a way to change the resonance behavior.

The 1 : 4 RS-DGS Divider Structure, and the transmission, reflection characteristics of the structure for varying defect lengths can be seen in Figure 26, and Figure 27 respectively.

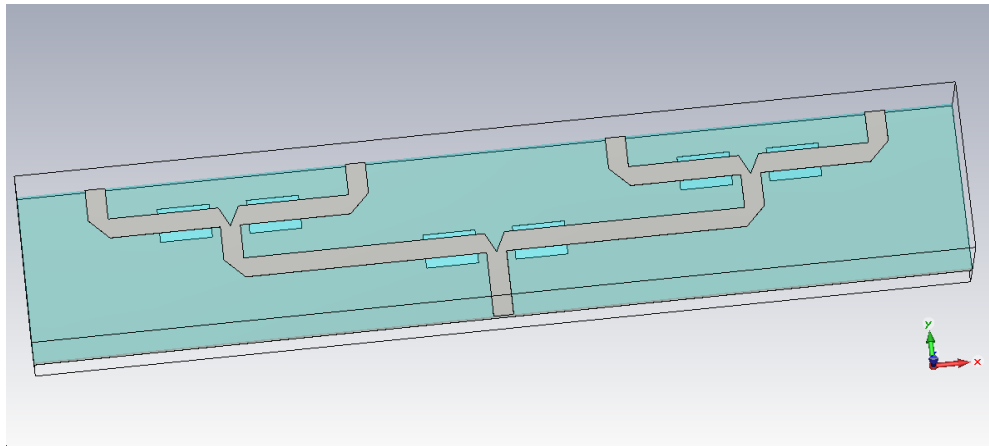


Figure 26. RS-DGS 1 : 4 Divider Structure.

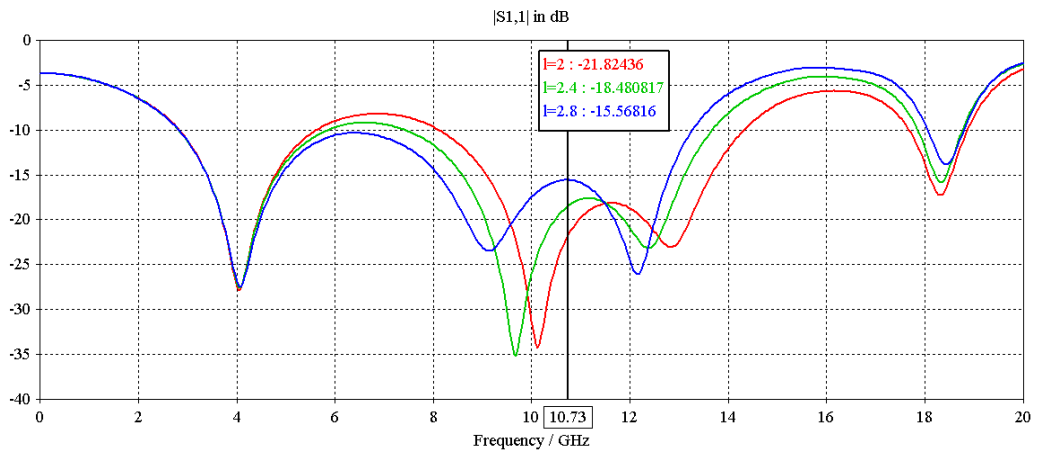


Figure 27.a. S_{11} of RS-DGS 1 : 4 Divider Structure for $d=0.5$, $w_d=2$, $l=2 : 0.4 : 2.8$ mm.

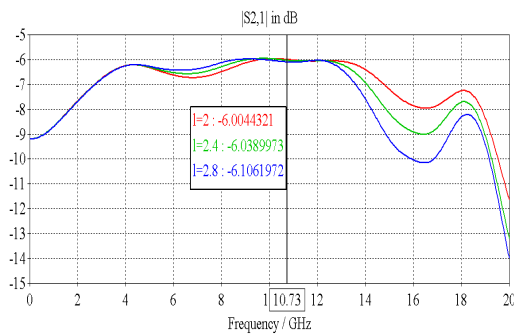


Figure 32.b. S_{21} of RS-DGS 1 : 4 Divider Structure for $d=0.5$, $w_d=2$, $l=2 : 0.4 : 2.8$ mm.

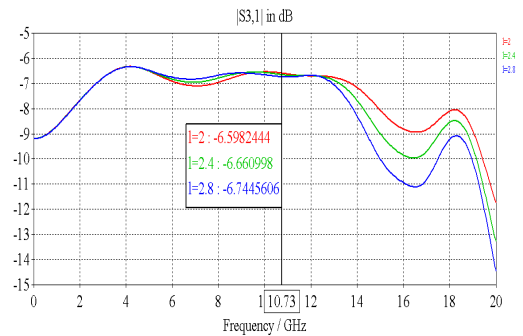


Figure 32.c. S_{31} of RS-DGS 1 : 4 Divider Structure for $d=0.5$, $w_d=2$, $l=2 : 0.4 : 2.8$ mm.

Contrary to the expectations, the change in the defect length does not change the resonant frequency. The change in the characteristics of the RS-DGS when used in cascade was also noted in an aperture coupled coupler structure. Trying the varying defect width, different defect lengths at the steps, or both different defect widths and lengths at the steps may also solve our problem, but these methods restrict the freedom of the designer, and is time-wasting. However, if the advantages of these methods are superior, these methods are worth trying.

Referring back to the reflection characteristics of the 1 : 4 structure, Figure 27, one can notice that there are two deeps in the 8 GHz -14 GHz band, and the maximum value is on the order of -15 dB, which calls out for a wideband divider structure that is worth trying the time-wasting simulation process. The first variable that comes to mind to vary is the defect width which may also cause a drop in the reflection. The resulting reflection characteristics for the varying defect width at different defect lengths ($l=2, l=3$ mm) can be seen in Figure 28.

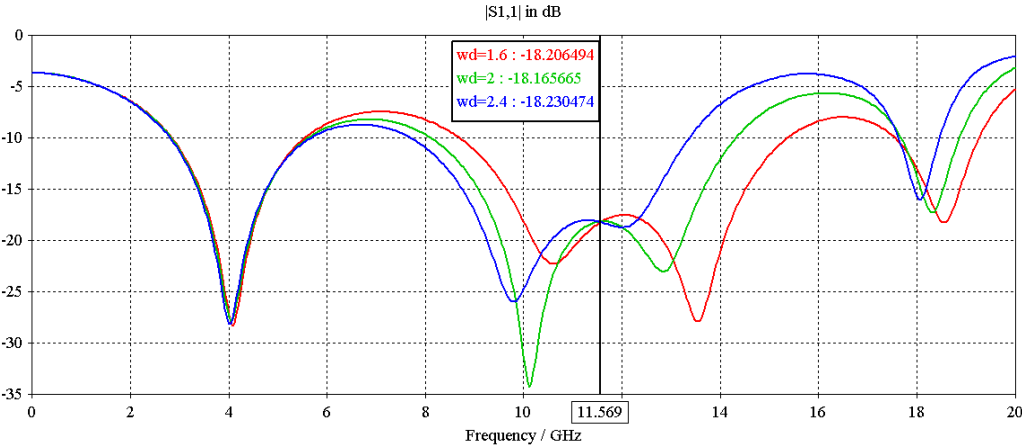


Figure 28.a. S_{11} for Varying Defect Width at $d=0.5, l=2$ mm.

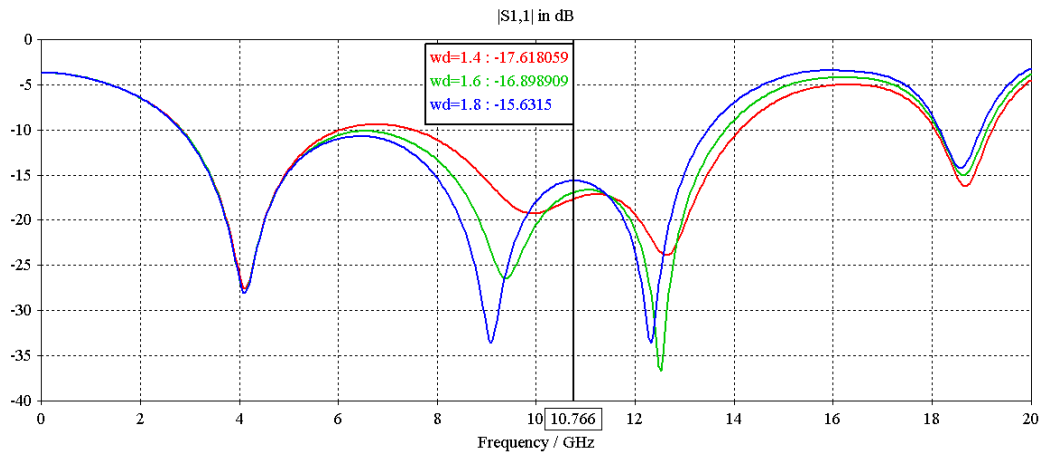


Figure 28.b. S_{11} for Varying Defect Width at $d=0.5$, $l = 3$ mm.

As the defect length increases, the resonance dips start to rise up. On the other hand, bandwidth increases. The best-fit values can be determined by means of the requirements of the design.

The structure seems like wideband with a maximum -16.7 dB reflection at the 8.4 GHz – 13.2 GHz band for 1.6 mm defect width (w_d), and 3 mm defect length (l). The transmission characteristics for the related structure are also stable in the 8.4 GHz – 13.2 GHz band:

$$S_{21}=S_{51}= -6.12 \text{ dB to } -6.28 \text{ dB} \quad 0.18 \text{ dB variation in } 8.4 \text{ GHz} - 13.2 \text{ GHz band}$$

$$S_{31}=S_{41}= -6.64 \text{ dB to } -6.85 \text{ dB} \quad 0.21 \text{ dB variation in } 8.4 \text{ GHz} - 13.2 \text{ GHz band}$$

The inequality between the 2nd (& 5th) port and 3rd (and 4th) port can be compensated by changing the defect widths (or the lengths) at the ports. Changing the port defect widths as:

$$w_{d2}= w_{d5}= 1.7 \text{ mm}, \quad \text{and} \quad w_{d3}= w_{d4}= 1.5 \text{ mm}$$

the power levels of the both four ports can be equalized. (See Figure 29.) The deviation of the S-parameters from the standard value is as follows:

$$S_{11} = -15 \text{ dB maximum at } 13.2 \text{ GHz, and } -17 \text{ dB local maximum at } 11.1 \text{ GHz}$$

$S_{21}=S_{51} = -6.33 \text{ dB to } -6.56 \text{ dB}$

0.23 dB variation in 8.4 GHz – 13.2 GHz band

$S_{31}=S_{41} = -6.40 \text{ dB to } -6.57 \text{ dB}$

0.17 dB variation in 8.4 GHz – 13.2 GHz band

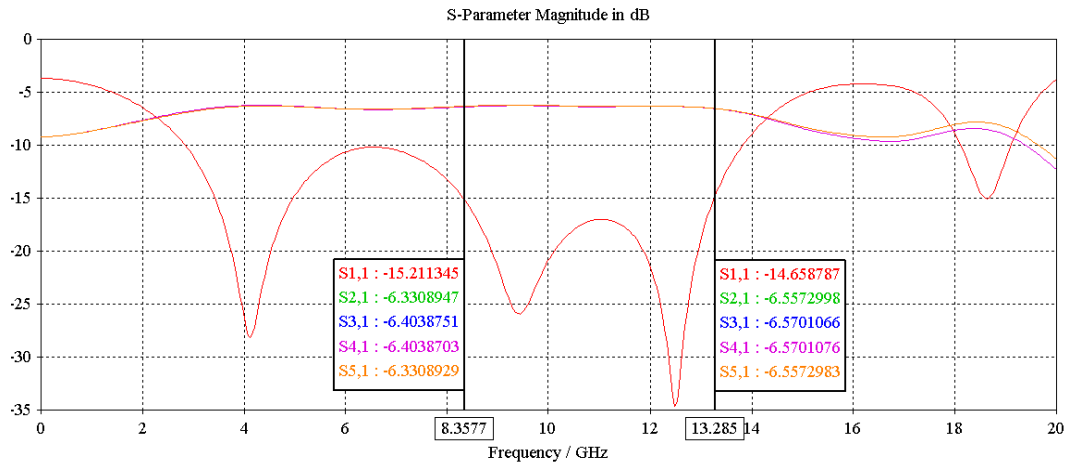


Figure 29. S-parameters of the 1 : 4 Divider with $w_d=1.6$, $w_{d2}=w_{d5}=1.7$, $w_{d3}=w_{d4}=1.5$, $l=3$, $d=0.5$ mm.

Also checking the phase of the transmission S-parameters is necessary. As can be seen from Figure 30, the phase difference between the ports is 1.6° maximum.

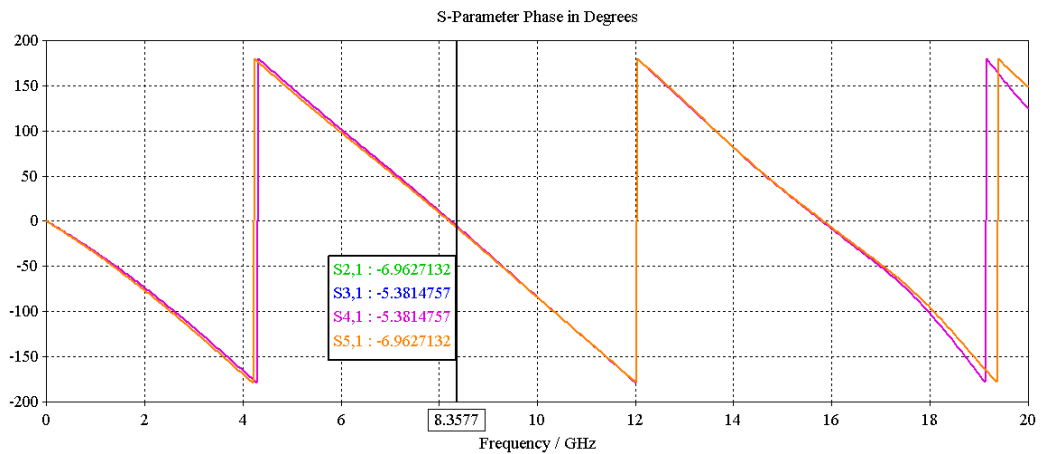


Figure 30. The Transmission Phase Characteristics in Degrees.

The 1 : 4 BFN centered at 10.5 GHz with a 24 % bandwidth has a superior performance with absolutely equal power division and good matching at the corresponding band, so moving one step further, the 1 : 8 BFN can also be designed at the X-band frequencies. Before proceeding to the 1 : 8 BFN, addition of a second dielectric beneath the 1 : 4 BFN is covered.

4.1.1 Addition of Dielectric Beneath the DGS

The transmission and reflection characteristics of the BFN designed by using DGS were promising due to the band-broadening properties. However, in order to measure the implemented BFN, the structure must be put into a metal box. The direct addition of the metal box under the DGS will short out the DGS, so the structure will lose its properties. So, the addition of dielectric under the DGS is necessary for packaging purposes. Even if a metal box is not necessary, the dielectric addition will control the radiation from the defect.

As a first step, addition of the second dielectric is monitored without the addition of a second ground. The previous studies on the dielectric addition state that the addition of a second ground beneath does not change the response. This situation will also be controlled by comparing the results of the two structures.

The effects of the dielectric addition has been investigated for 1 : 2 (T-junction) structure. The effects on the 1 : 4 is investigated.

The 1 : 4 structure with the related parameters can be seen in Figure 31.

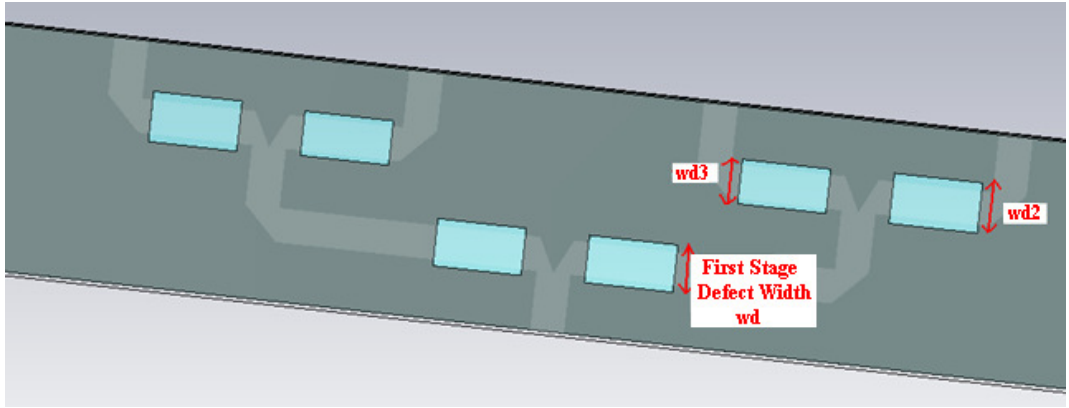


Figure 31. DGS 1 : 4 BFN.

The structure is symmetric with respect to the feed point. After the addition of the standard thickness (20 mil) dielectric under the DGS, the structure is simulated with the previously chosen parameters ($l=3$ mm, $w_{d3}+0.1=w_{d2}-0.1=w_d$ mm). The simulation is done for varying w_d ($w_d=1.4, 1.6,$ and 1.8 mm). The corresponding results can be seen in Figure 32.

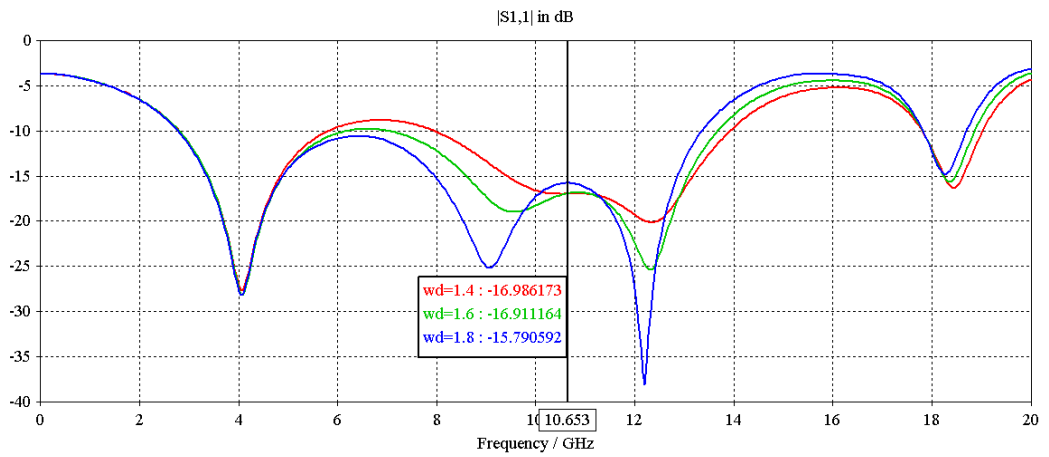


Figure 32.a. S_{11} for 1 : 4 Divider with $l = 3$, $w_d = 1.4 : 0.2 : 1.8$ mm ($w_d = w_{d2} - 0.1 = w_{d3} + 0.1$).

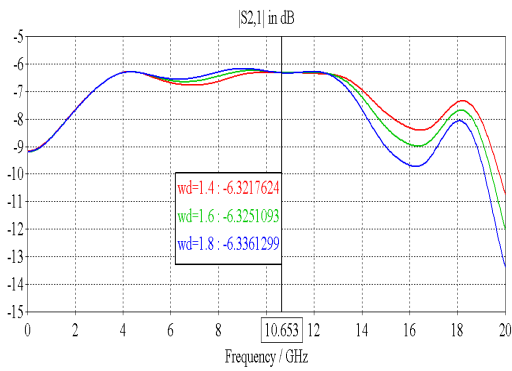


Figure 32.b. S_{21} for 1 : 4 Divider with $l = 3$, $w_d = 1.4 : 0.2 : 1.8$ mm ($w_d = w_{d2} - 0.1 = w_{d3} + 0.1$).

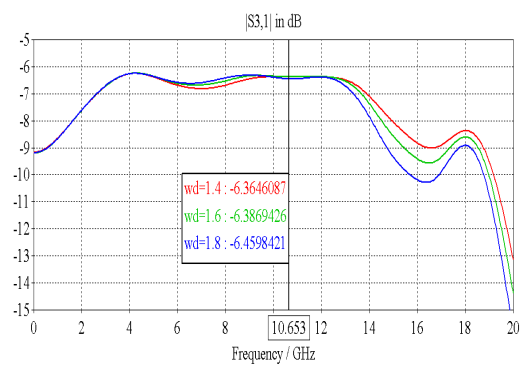


Figure 32.c. S_{31} for 1 : 4 Divider with $l = 3$, $w_d = 1.4 : 0.2 : 1.8$ mm ($w_d = w_{d2} - 0.1 = w_{d3} + 0.1$).

One variation that might be worth trying is the variation of the second stage defect widths (w_{d2} , and w_{d3}) while keeping the first stage defect width same ($w_d = 1.6$ mm). The results for the corresponding structure can be seen in Figure 33.

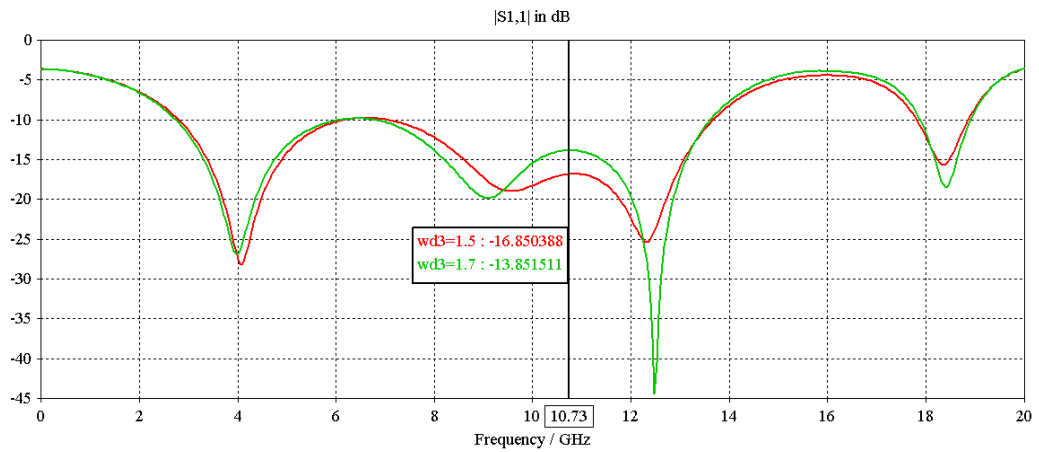


Figure 33.a. S_{11} for 1 : 4 Divider with $l = 3$, $w_d = 1.6$, $w_{d3} = 1.5, 1.7$ mm ($w_{d2} = w_{d3} + 0.2$).

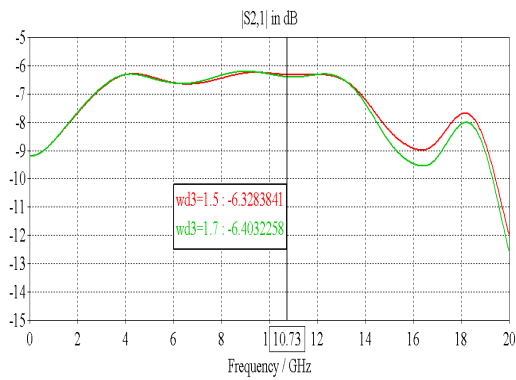


Figure 33.b. S_{21} for 1 : 4 Divider with $l = 3$, $w_d = 1.6$, $w_{d3} = 1.5, 1.7$ mm ($w_{d2} = w_{d3} + 0.2$).

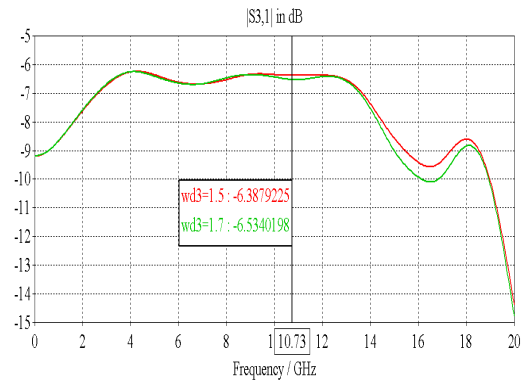


Figure 33.c. S_{31} for 1 : 4 Divider with $l = 3$, $w_d = 1.6$, $w_{d3} = 1.5, 1.7$ mm ($w_{d2} = w_{d3} + 0.2$).

It would have been necessary to monitor the change in the defect length (l) to see the effects of the change on the response of the BFN. However, the simulations done for $l = 3.25$ mm has shown no significant change from the $l = 3$ mm case.

The results with the second ground added beneath can be seen in Figure 34.

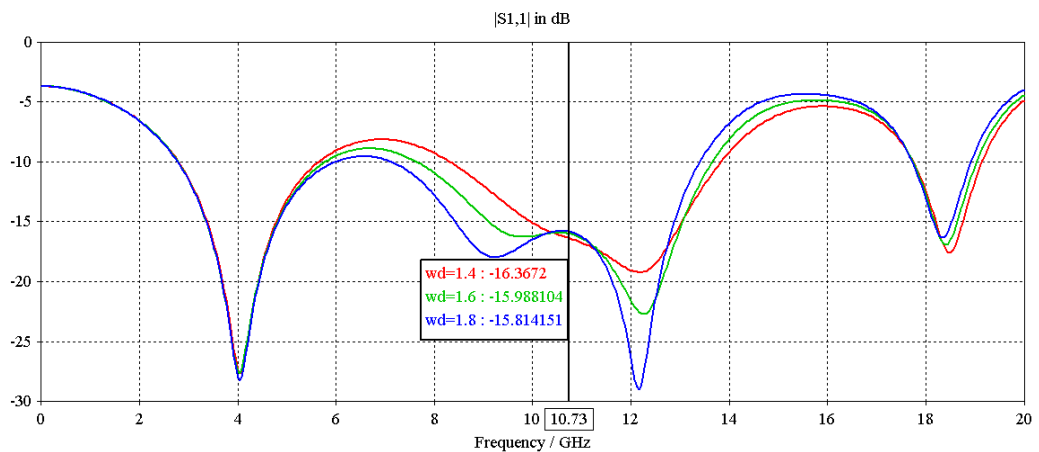
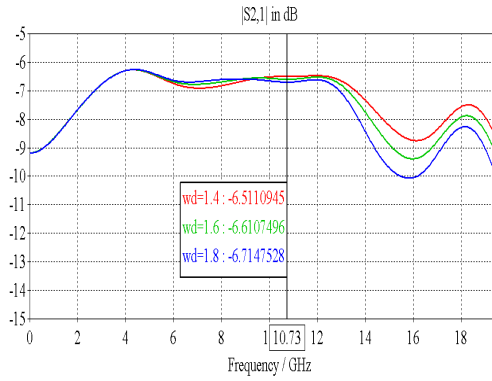


Figure 34.a. S_{11} for 1 : 4 Divider with $l = 3$, $w_d = 1.4 : 0.2 : 1.8$ mm ($w_d = w_{d2} - 0.1 = w_{d3} + 0.1$) After the Addition of the Second Ground.



4.1.2

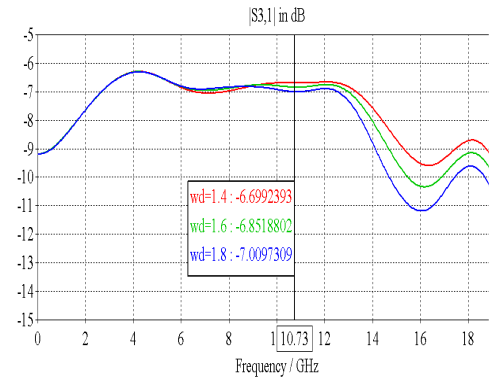


Figure 34.b. S_{21} for 1 : 4 Divider with $l = 3$, $w_d = 1.4 : 0.2 : 1.8$ mm ($w_d = w_{d2} - 0.1 = w_{d3} + 0.1$) After the Addition of the Second Ground.

Figure 34.c. S_{31} for 1 : 4 Divider with $l = 3$, $w_d = 1.4 : 0.2 : 1.8$ mm ($w_d = w_{d2} - 0.1 = w_{d3} + 0.1$) After the Addition of the Second Ground.

Comparing the results in Figure 32 and Figure 34, it can be deduced that the addition of the 2nd ground beneath the 2nd dielectric does not significantly affect the resulting S-parameters.

From the all above results, the chosen is 1 : 4 divider with:

$$l = 3, w_d = 1.8, w_{d2} = 1.9, \text{ and } w_{d3} = 1.7 \text{ mm.}$$

However, the magnitudes of S_{21} and S_{31} are a slightly different for these values. These values are in the range of:

$$S_{21} = 6.50 \text{ dB} - 6.65 \text{ dB} \quad \text{and} \quad S_{31} = 6.70 \text{ dB} - 6.85 \text{ dB.}$$

The difference between these S_{21} and S_{31} values can be equalized by making small changes at the port-level defect widths. The resulting structure and the corresponding S-parameters can be seen in Figure 35.

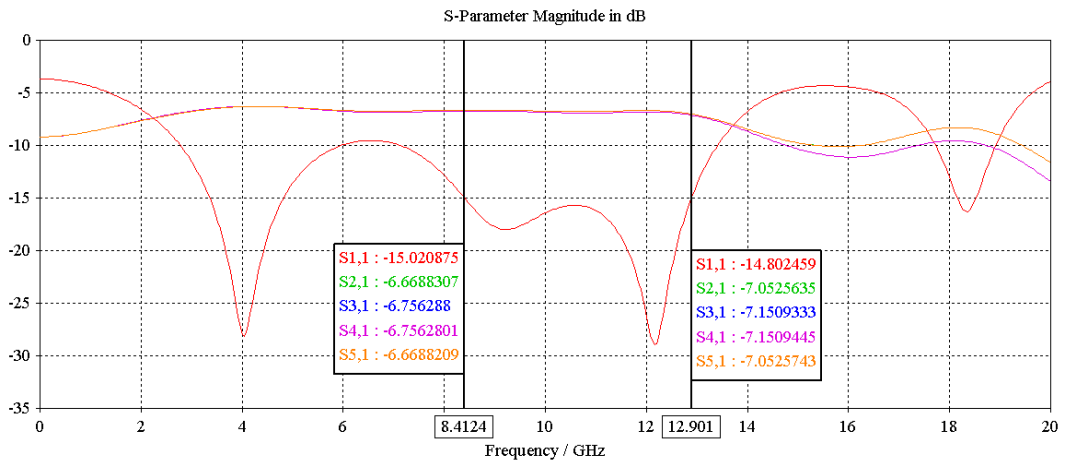


Figure 35.a. S-parameters for the Resulting 1 : 4 BFN with 10 mm Distance between Ports ($l=3$, $d=0.5$, $w=1.15$, $w_d=1.8$, $w_{d2}=1.95$, $w_{d3}=1.65$ mm).

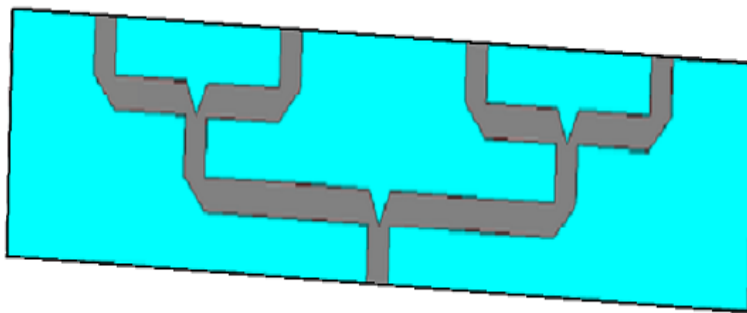


Figure 35.b. The Resulting 1 : 4 BFN Upper View (Port Numbering Starts with #2 from the Right).

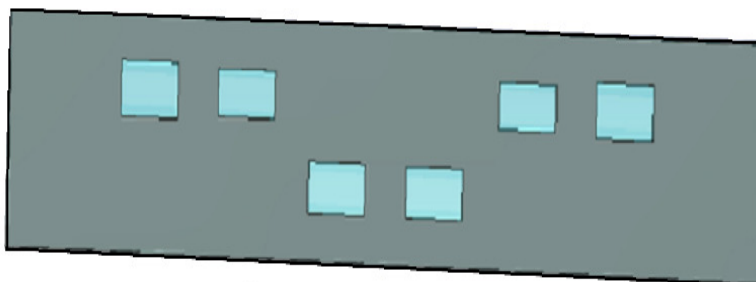


Figure 35.c. The Resulting 1 : 4 BFN Ground View.

The designed 1 : 4 BFN has 10 mm distance between two ports which corresponds to $0.33\lambda_0$ where λ_0 is the free-space wavelength (30 mm at 10 GHz). This distance is generally set to a value greater than $0.5\lambda_0$ in order to avoid grating lobes. As a rule of thumb, this distance is set to $0.7\lambda_0$ and the resulting structure is simulated with no other parameter changes. The resulting 1 : 4 BFN with the corresponding structural view, parameters, and S-parameters can be seen in Figure 36.

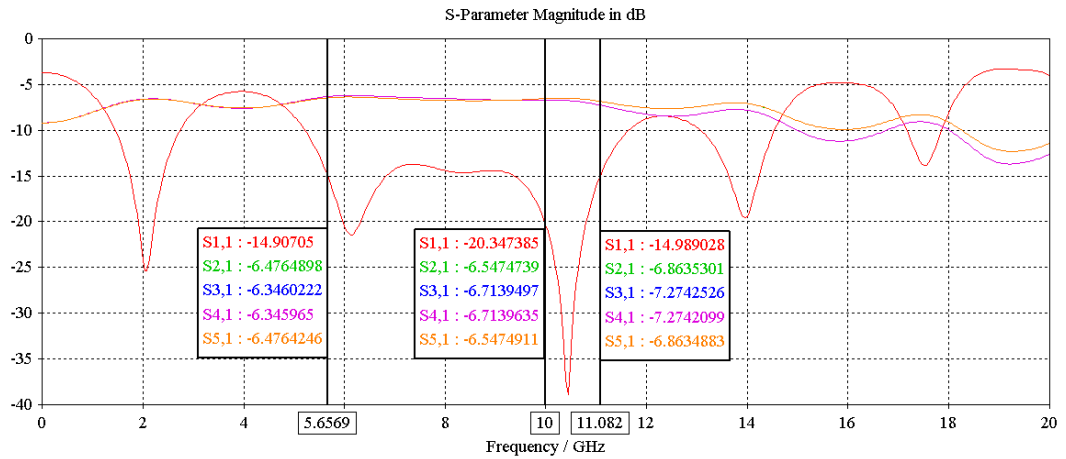


Figure 36.a. S-parameter Magnitude Values for the Resulting 1 : 4 BFN with 21 mm Spacing ($0.7\lambda_0$) Between Two Ports ($w=1.15$, $l=3$, $d=0.5$, $l_0=21$, $wd=1.8$, $wd_2=wd_5=2$, $wd_3=wd_4=1.6$ mm).

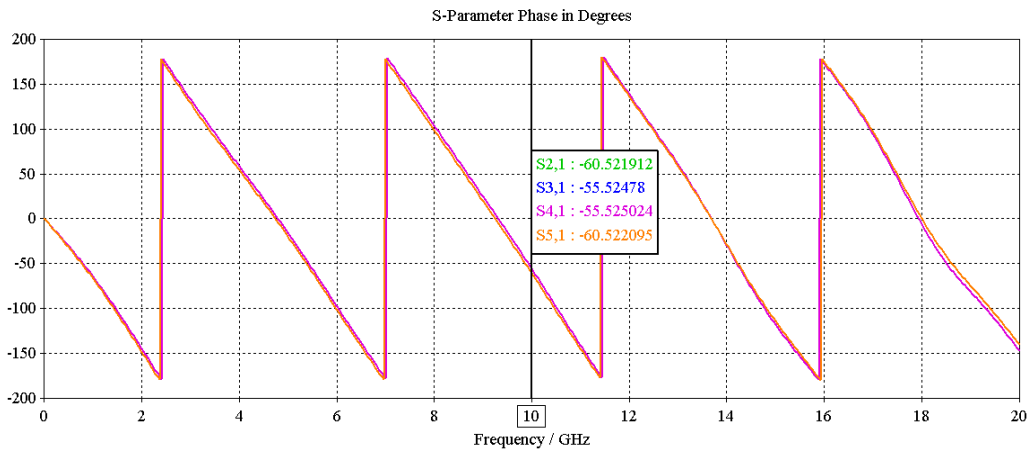


Figure 36.b. S-parameter Phase Values for the Resulting 1 : 4 BFN with 21 mm Spacing ($0.7\lambda_0$) Between Two Ports ($w=1.15$, $l=3$, $d=0.5$, $l_0=21$, $wd=1.8$, $wd_2=wd_5=2$, $wd_3=wd_4=1.6$ mm).

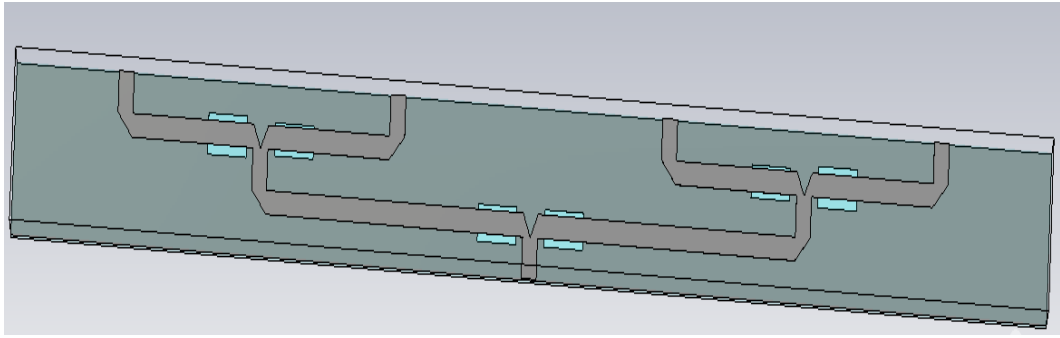


Figure 36.c. The Resulting 1 : 4 BFN (Port Numbering Starts with #2 from the Right).

Since the structure is now in its final shape, the total loss of the structure can be calculated for the entire 5.6 GHz – 11 GHz frequency band. However, due to the stability of the S-parameters, calculation of loss at 10 GHz will give us enough insight.

At 10 GHz, $S_{11}=-20.35$, $S_{21}=S_{51}=-6.55$, $S_{31}=S_{41}=-6.71$ dB. The dissipated power in dB can be found as:

$$P_{loss\ dB} = 10 \times \log \left(\frac{1}{\left(10^{\frac{S_{11}}{10}} + 10^{\frac{S_{21}}{5}} + 10^{\frac{S_{31}}{5}} \right)} \right) = 10 \times \log \left(\frac{1}{0.878} \right)$$

$$= 10 \times \log (1.1384) = 0.56\ dB\ at\ 10\ GHz$$

The loss factors show that a significant loss is not introduced into the system from the defects. This claim can be verified by checking the per meter loss of the microstrip line at 10 GHz which is 3.6 dB/m. This is the per meter loss due to the dielectric and conductor losses. Considering the total length of the structure, 12.8 cm, the total loss due to these two factors comes out to be 0.55 dB. Hence, it is obvious that the radiation due to the defect is not a loss factor, or the insertion of defect into the system boost the loss.

4.1.2 Implementation of the DGS 1 : 4 BFN

The simulated DGS 1 : 4 BFN is implemented by using the LPKF 6 mil Cutter. The process of the upper layer and three of the defect openings was done by the 6 mil End-Mil Cutter. However, due to the stiffness of the End-Mil Cutter, the remaining three defect openings could not be done by the End-Mil Cutter, instead were done by the Universal Cutter of the same preciseness. This non-standard cutter selection can result in the decrement of the symmetry of the device.

Before the production process, another change was also necessitated in order to keep the length width ratio of the resulting device in a proper range. In the resultant 1 : 4 BFN design, feed ports and the distance between two parallel lines were set as 2 mm resulting in approximately 8 mm total device width which is difficult to handle. Since, the distance between the two parallel lines is a determining factor, it has to be kept the same. Hence, the length of the feed ports is changed. Another reason for extending the feed ports is that, there has to be enough space for the connectors to be placed at the ports. The connectors used are Board Edge SMA Connectors which has a 1 cm x 0.3 cm dimensions. The dimensions are the length values parallel, and perpendicular to the port feeds respectively. Resulting dimensions of the feed ports are arranged as 16.7 mm for the 1st port, and 4 mm for the remaining. The corresponding structure and the related simulation results can be seen in Figure 37.

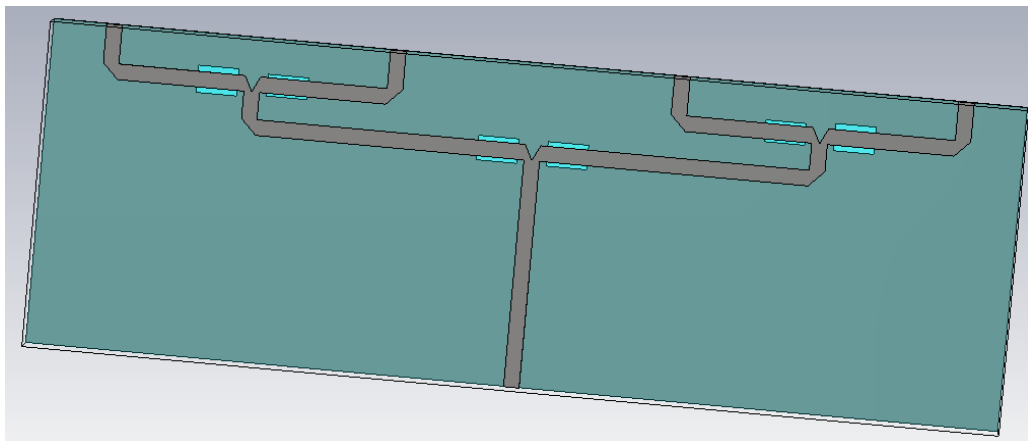


Figure 37.a. The Implemented DGS 1 : 4 BFN.

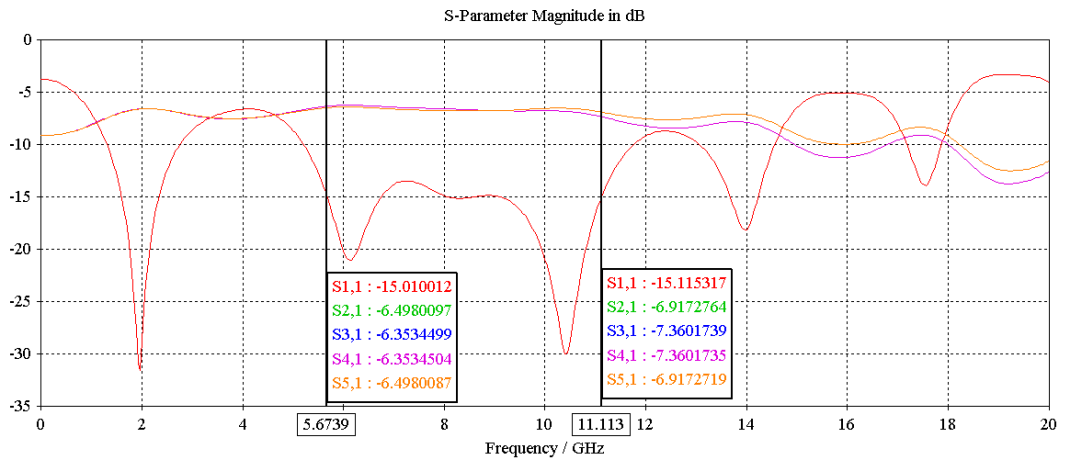


Figure 37.b. S-Parameters for the Implemented DGS 1 : 4 BFN.

The results for the DGS 1 : 4 BFN has not been affected by the change in the port lengths since the change is done by monitoring the previous results.

Since plot data can be given to LPKF in the form of dxf, which can be realized by ADS Momentum; ADS Momentum is used for plotting the device to be cut and graved. The corresponding ADS Momentum view and the results can be seen in Figure 38. The circles on the substrate are screw slots which are used for the purpose of holding the two substrates together.

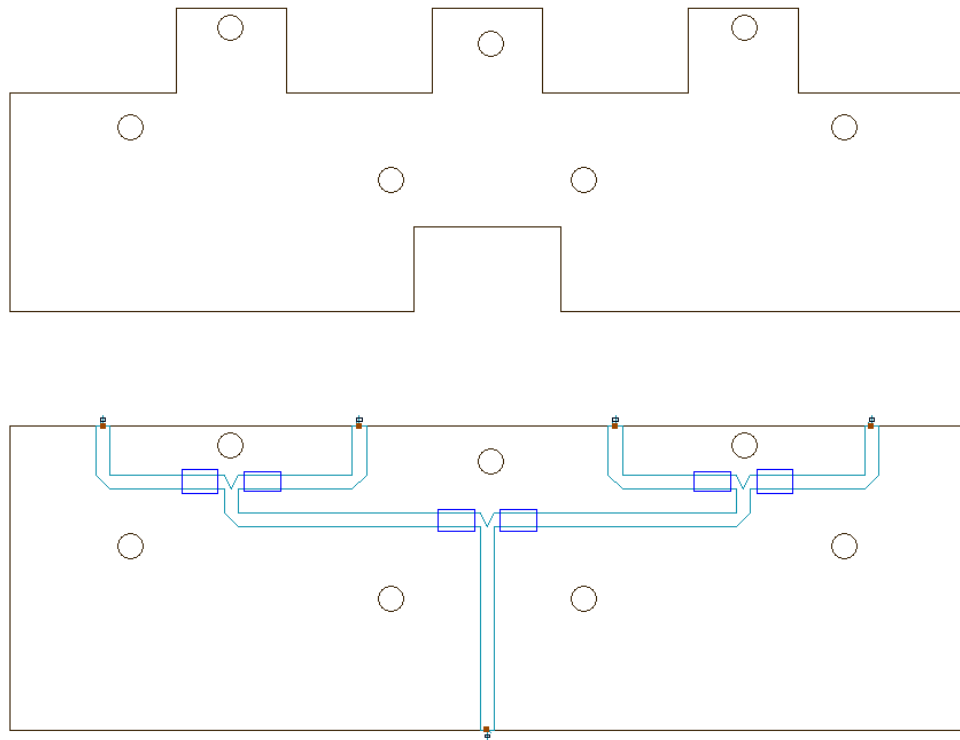


Figure 38. a. The Implemented DGS 1 : 4 BFN in ADS Momentum.

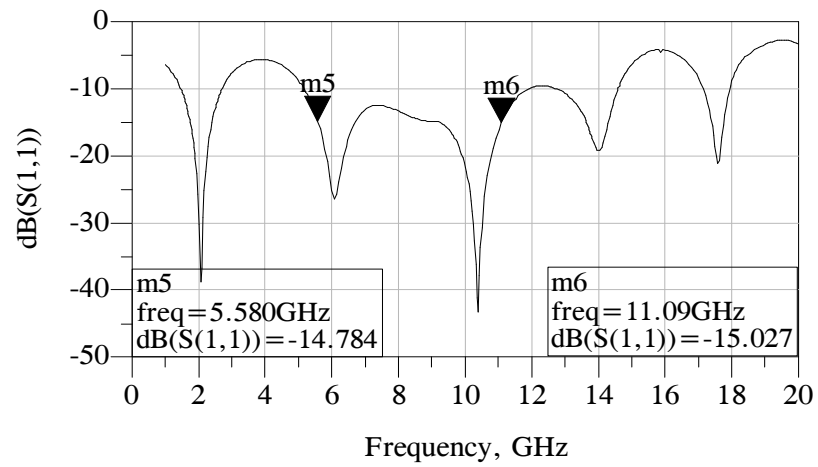


Figure 38.b. Reflection Parameters for the DGS 1 : 4 BFN in ADS Momentum.

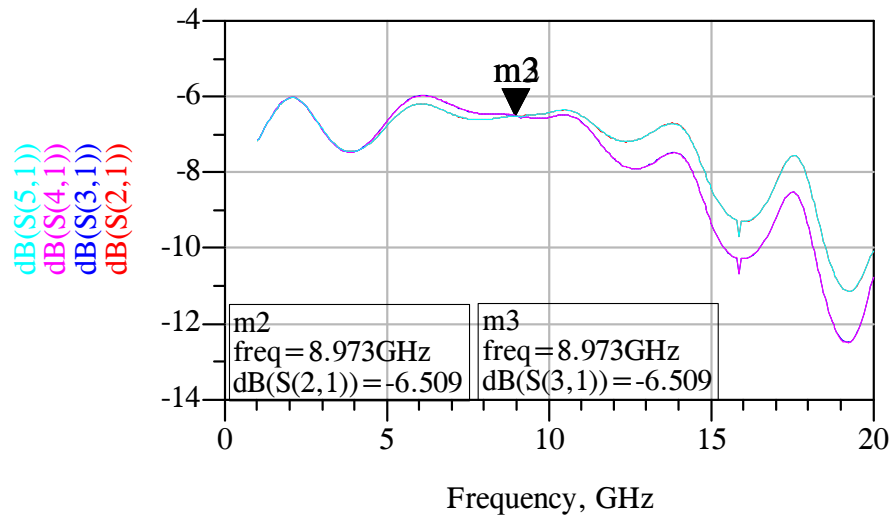


Figure 38.c. Transmission Parameters for the DGS 1 : 4 BFN in ADS Momentum.

The simulation results of the CST MICROWAVE STUDIO® and the ADS Momentum are also consistent showing a matching level below 15 dB in the 5.6 GHz – 11.1 GHz. The power levels at the output ports are also consistent at the neighborhood of 6.5 dB and 6.7 dB at 10 GHz. Thus, the simulation programs confirm each other which is a factor that encourages the designer that the measurements will also be in harmony with the simulation results.

The DGS 1 : 4 BFN is produced at the Millimeter wave Laboratory of the Department of Electrical and Electronics, METU with the guidance of Erdinç Yurdakul. The produced two-layer structure in the final form and with its all four faces can be seen in Figure 39.

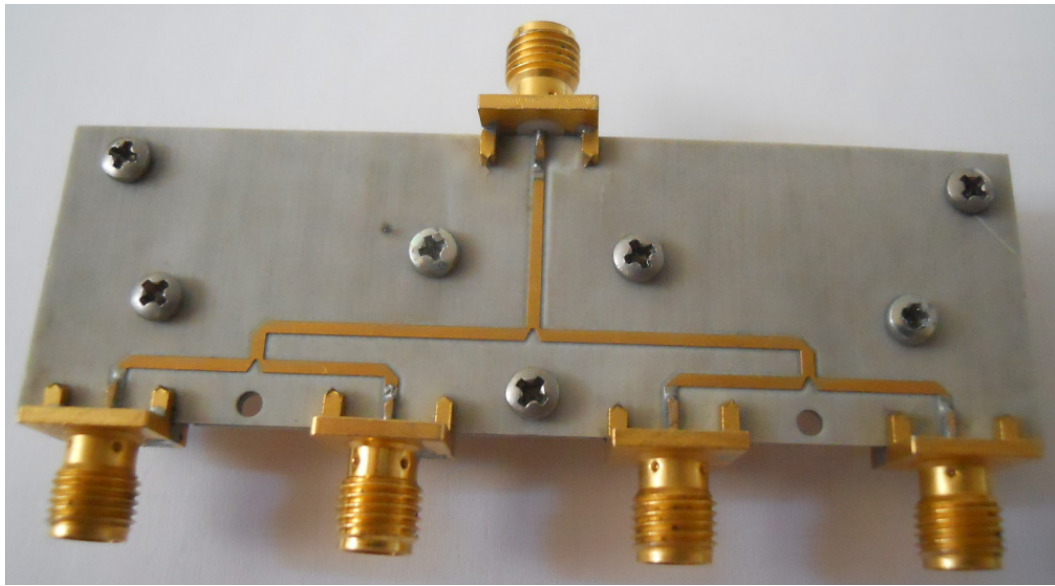


Figure 39.a. The General View of the Produced 1 : 4 DGS BFN.

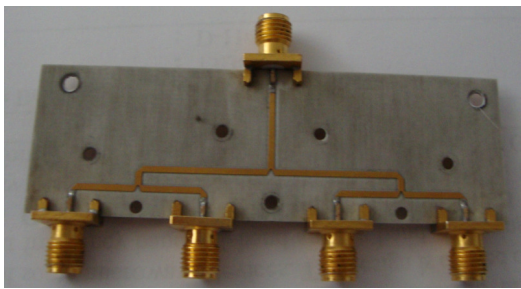


Figure 39.b. Front Face of the Upper Layer.

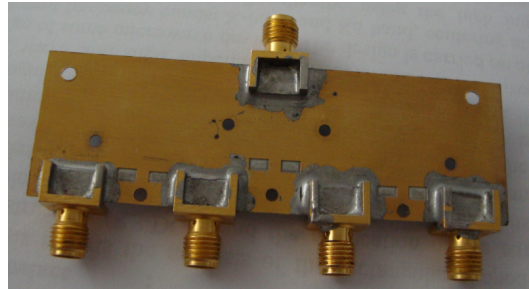


Figure 39.c. Back Face of the Upper Layer.



Figure 39.d. Front Face of the Lower Layer.

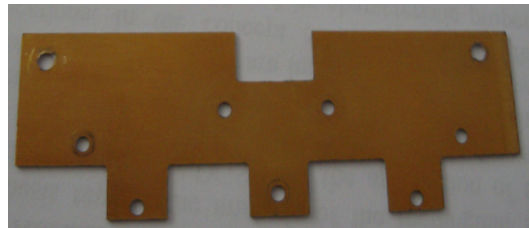


Figure 39.e. Back Face of the Lower Layer.

The produced device is measured at the Microwave Education Laboratory with HP E5071C Series Network Analyzer in the 5 GHz – 13 GHz range, and the corresponding magnitude results can be seen in Figure 40.

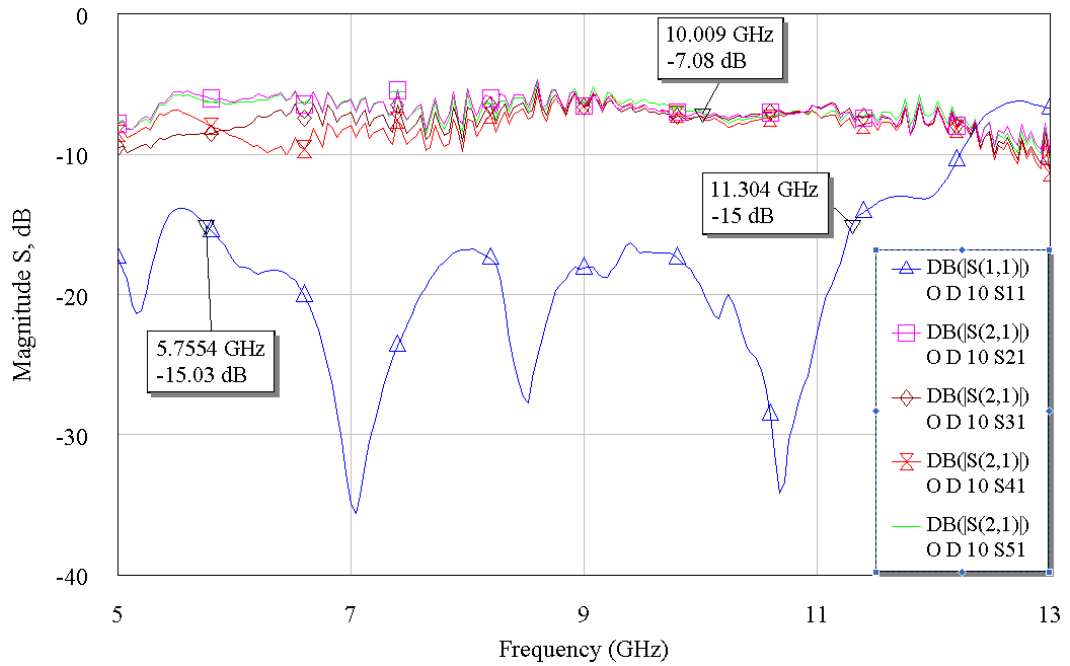


Figure 40. Measurement Results of the DGS 1 : 4 BFN.

The measurement results include the undesired effects of the connectors, and the multi reflections from these connectors. Resultantly, an impure output is concluded which is difficult to compare with the simulation results. In order to get rid of these undesired impacts, time domain gating (TDG) property of the network analyzer is suitable.

Shortly explaining the TDG progress; the standard calibration is done, and the device under test (DUT) is measured for its S-parameters, then the resulting S-parameter measurement is transformed into a time domain signal which shows the response of the total system. The desired response can be selected here by using the TDG. Hence, the other, undesired responses can be filtered out, and this time domain response can be transformed back into the frequency domain. This process also permits the comparison of the simulation and the measurement results.

TDG is processed at the E8361A PNA Network Analyzer at the Millimeter wave Laboratory in the 5 GHz – 13 GHz band, and the corresponding (both the phase and the

magnitude) results can be seen in Figure 41. Note that the port 2 & 5, and 3 & 4 are symmetric, so these four ports are denoted only by Ports # 2 & 3.

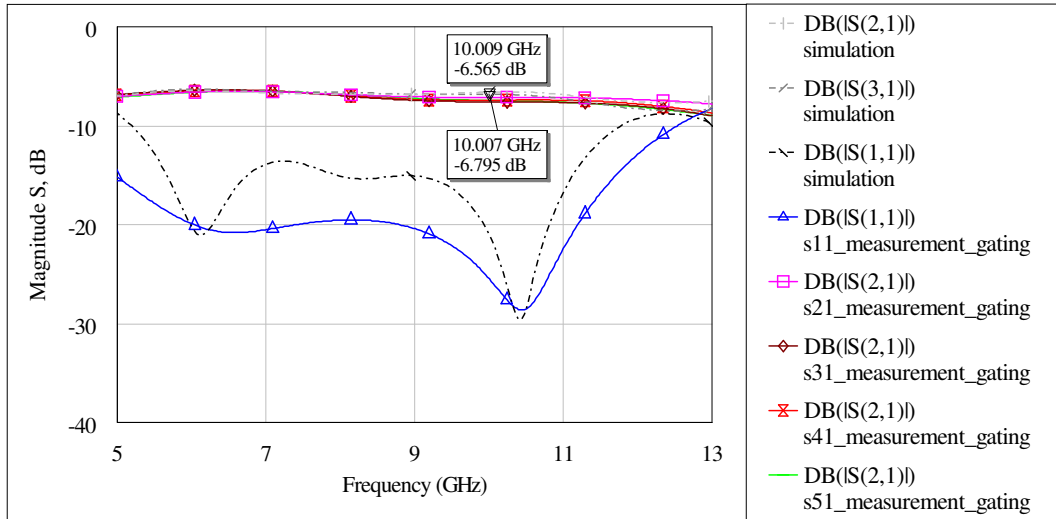


Figure 41.a. S-parameter Magnitude Values for the Simulation and the Measurement.

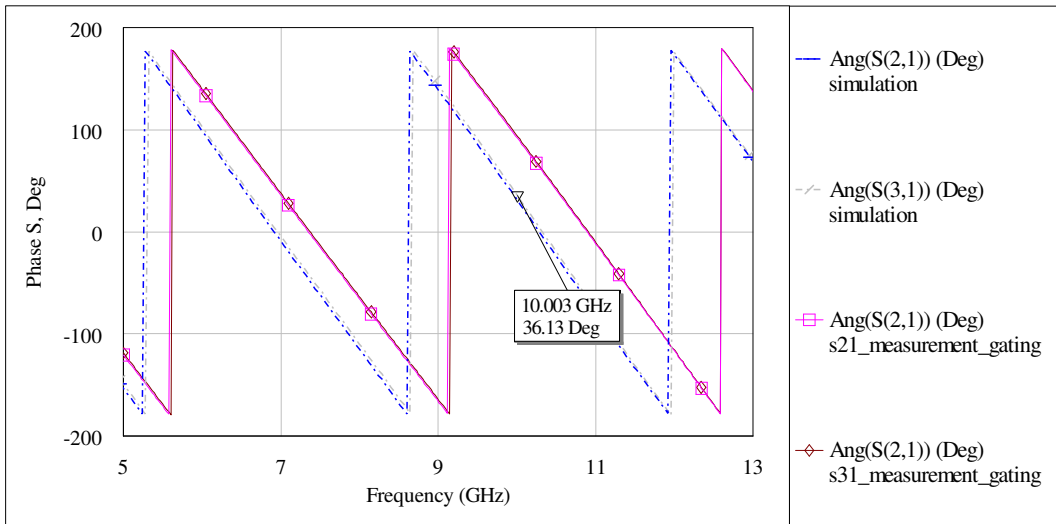


Figure 41.b. S-parameter Phase Values for the Simulation and the Measurement.

The measurement results are in harmony with the simulation results. S_{11} magnitude is below the simulation value in the 5.6 GHz – 11.1 GHz band. The power distribution between the output ports are at good correspondence. At 10 GHz, output port power is -6.8 dB. This level is acceptable since the level at the simulation was -6.56 dB.

S-parameter phase values are 3° apart according to the simulation results, and this difference is extended to 8° at the measurement which is still acceptable in this study.

4.2 DGS 1 : 8 BFN Design

The 1 : 8 BFN is again in the compact form as seen from the upper view in Figure 42. The defect-related parameters are optimized in order to find the best-match condition. At the design procedure, 3rd order defect widths, which are the ones nearest to the ports will again be employed in order to equalize the port powers. The corresponding defect widths are named as w_{di} ($i=2,3,4,5$) where i corresponds to the related port number, and there exists symmetry with respect to the feeding point (Port # 1) which means, $w_{di}=w_{d(11-i)}$, i.e., $w_{d2}=w_{d9}$ etc.

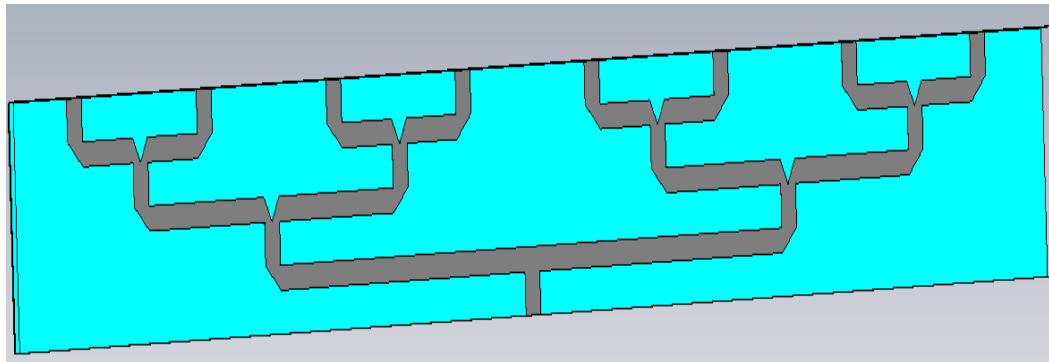


Figure 42. The Upper View of the DGS 1 : 8 BFN.

The previous studies on the DGS 1 : 4 divider has shown us that the increase in the defect length results in a decrease in the reflection. However, it also causes a decrease in the bandwidth.

It would be helpful for the 1 : 8 divider to check the effect of defect length first, and then choosing the proper defect length, deciding on the defect width is necessary. One can see the effect of varying defect length by checking Figure 43.

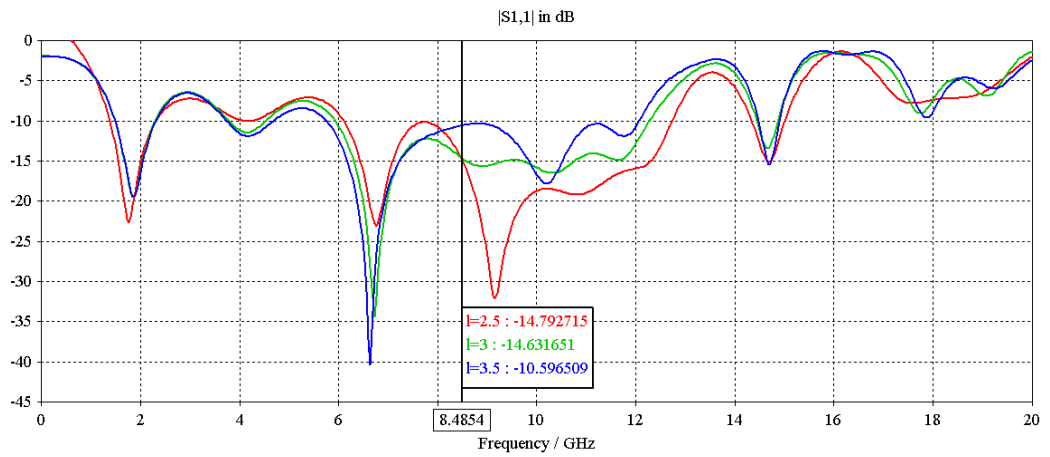


Figure 43. S-parameters for $d=0.5$, $w_d=2$, $l=2.5 : 0.5 : 3.5$ mm.

Considering Figure 43, it would be wise to choose the defect length as 2.5 mm. Now, setting defect length constant, vary the defect width in order to find the best match condition.

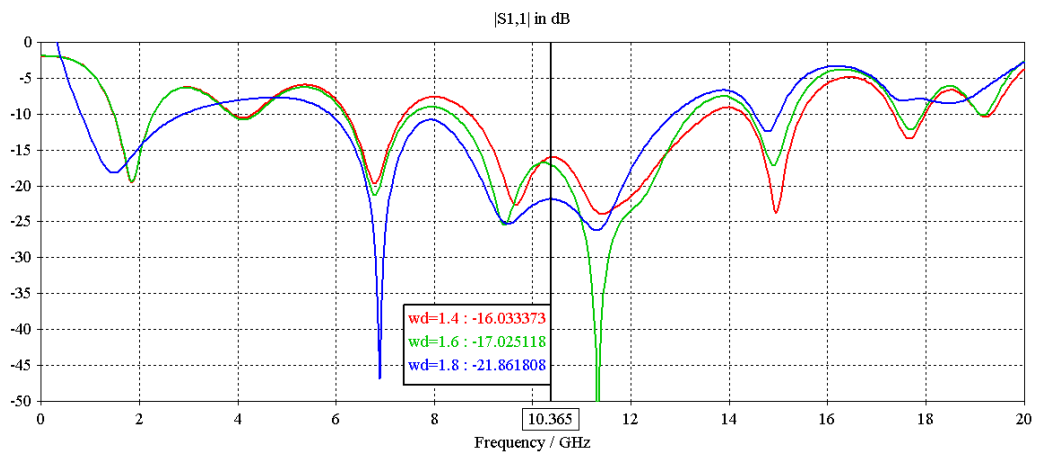


Figure 44.a. S_{11} for $l=2.5$, $d=0.5$, $w_d=1.4 : 0.2 : 1.8$ mm.

Inspiring from Figure 44, defect width is chosen as 1.8 mm since the S_{11} shows the most stable response. Considering the design with 1.8 mm defect width, it is also expected that

the ports do not receive equal power due to the different coupling factors of the lines feeding the ports. Thus, it would be convenient to state that the defect widths at different ports should be varied in order to equalize the port powers. The defect width at the ports which receive less power than the expected is decreased and the reverse is done for the ports that receive more power than the expected. The new results with equal port power are shown in Figure 45 with the corresponding defect widths (w_d) given.

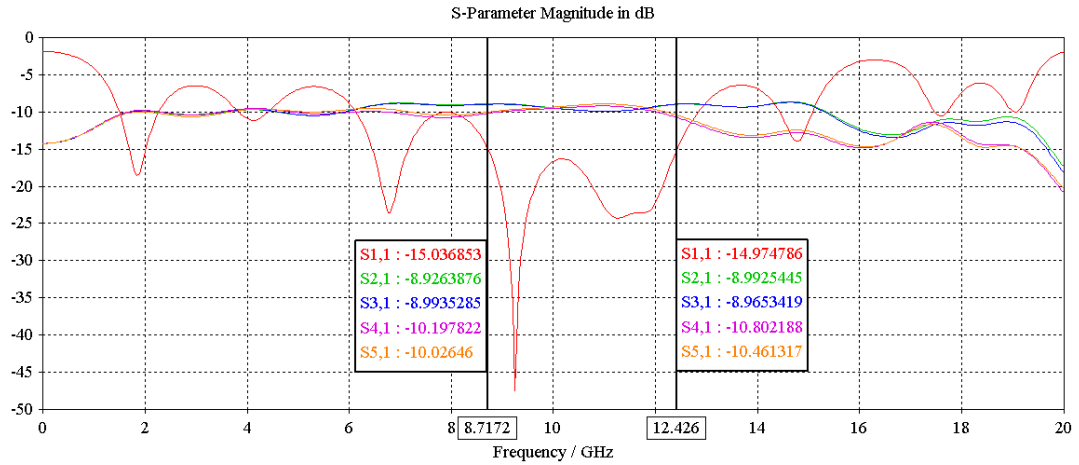


Figure 45. S-parameters for the Defect Widths $w_{d1}=1.8$, $w_{d2}=1.5$, $w_{d3}=1.3$, $w_{d4}=2.1$, $w_{d5}=2.3$ mm.

Note that the S-parameters of the remaining ports (ports 6, 7, 8, and 9) are not shown due to the symmetry, i.e. : $S_{21}=S_{91}$, $S_{31}=S_{81}$, $S_{41}=S_{71}$, and $S_{51}=S_{61}$.

The transmitted power to the ports is not as close as the 1 : 4 case. Note that a maximum deviation of 2 dB is possible between the ports. However, this does not play an important role in the defined bandwidth. One can equalize the transmitted power of the ports by simply changing the port defect widths in the 8.7 GHz – 12.4 GHz band.

4.2.1 Addition of Dielectric Beneath the DGS

Stemming from the previous experiences of the dielectric addition, it can be stated that the only critical consequence may be the shift of the frequency band which can be handled if the shift is not superior. The DGS 1 : 8 BFN with the the 2nd dielectric added and the remaining parameters same can be seen in Figure 46 with the corresponding results.

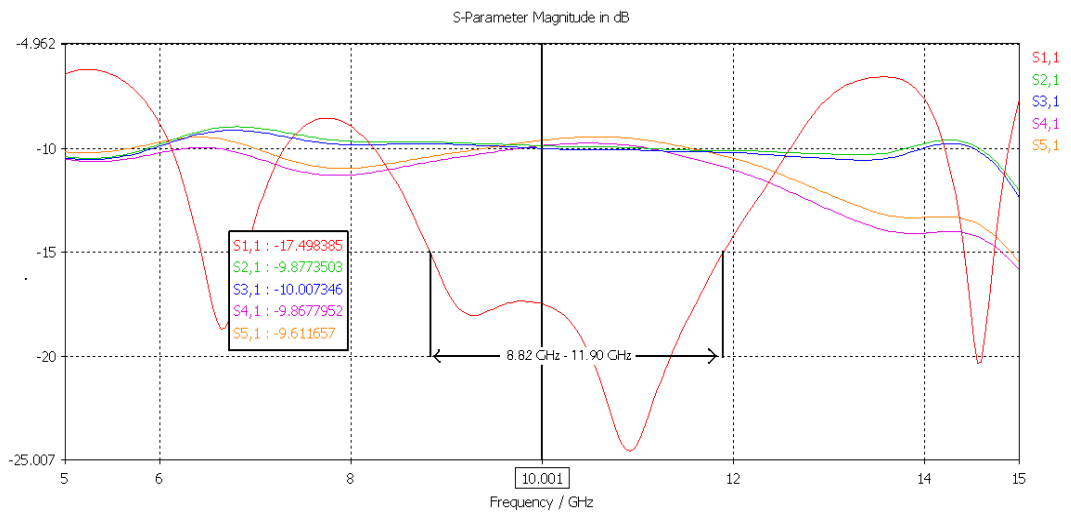


Figure 46.a. S-parameters for the Resulting 1 : 8 BFN with 10 mm Distance between Ports ($l=2.5$, $d=0.5$, $w=1.15$, $w_d=1.8$, $w_{d2}=1.5$, $w_{d3}=1.3$, $w_{d4}=2.1$, $w_{d5}=2.3$).

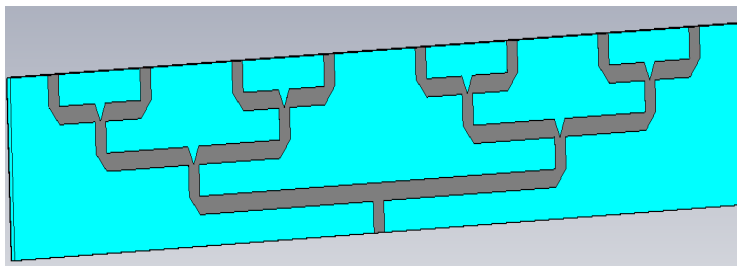


Figure 46.b. The Resulting 1 : 8 BFN Upper View (Port numbering starts with #2 from the right).

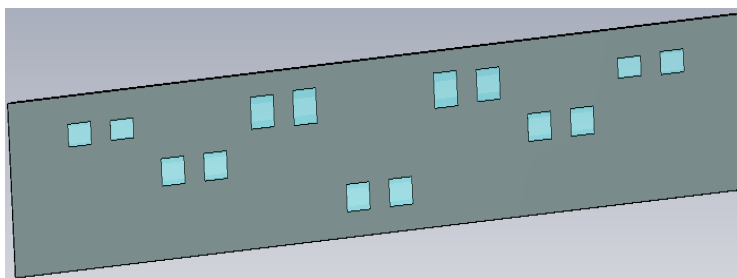


Figure 46.c. The Resulting 1 : 8 BFN Upper View.

The 1 : 8 BFN is also modified in order to have $0.7 \cdot \lambda_0$ distance between the two ports. The corresponding structure and the S-parameters can be seen in Figure 47.

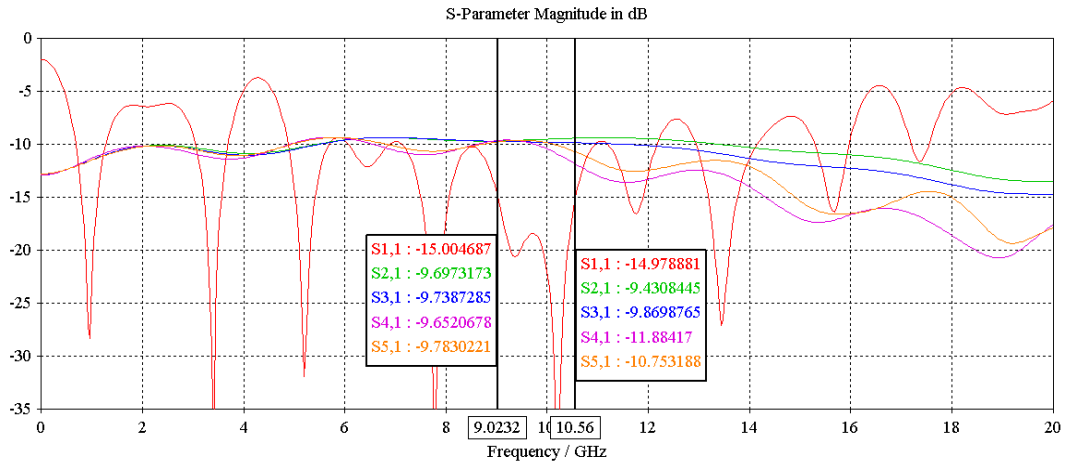


Figure 47.a. S-parameters for the Resulting 1 : 8 BFN with 21 mm Spacing ($0.7 \cdot \lambda_0$) Between Two Ports ($w=1.15$, $l=2.5$, $l_0=21$, $w_d=w_{d1}=1.8$, $w_{d2}=w_{d9}=1.5$, $w_{d3}=w_{d8}=1.3$, $w_{d2}=w_{d9}=2.1$, $w_{d3}=w_{d8}=2.3$ mm)..

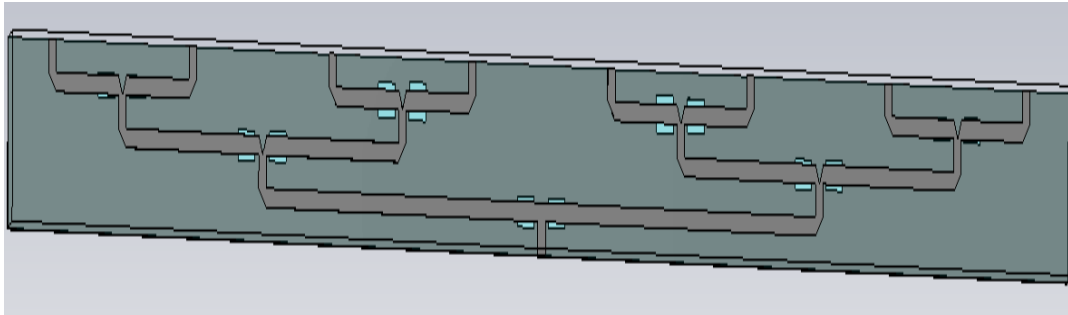


Figure 47.b. The Resulting 1 : 8 DGS BFN (Port numbering starts with #2 from the right).

At 10 GHz, $S_{11}=-22.06$, $S_{21}=S_{91}=-9.53$, $S_{31}=S_{81}=-9.82$, $S_{41}=S_{71}=-10.47$, $S_{51}=S_{61}=-9.86$ dB.

The total dissipated power can be found as :

$$P_{loss\ dB} = 10 \times \log \left(\frac{1}{\left(10^{\frac{S_{11}}{10}} + 10^{\frac{S_{21}}{5}} + 10^{\frac{S_{31}}{5}} + 10^{\frac{S_{51}}{5}} \right)} \right) = 10 \times \log \left(\frac{1}{0.82} \right)$$

$$= 10 \times \log (1.21) = 0.84\ dB\ at\ 10\ GHz$$

4.3 BFN at Millimeter-wave Frequencies

BFN design is revealed at X-band with the usage of Rogers R4003C substrate. The new task is to repeat the same design procedure at 35 GHz. However, Rogers4003C substrate is not convenient to be used at this frequency due to the dielectric losses. There are two alternatives on which the standard BFN designs studies have been conducted. These alternatives are the CuFlon and the Alumina substrates.

Due to the increase in the frequency, the length components will start to decrease. So, a reduction in the transmission line parameters is also necessary. The associated parameter is the line width which is essentially reduced. The other parameters such as defect width, or the distance between the ports (l_o) will also be directly lessened. However, the distance between the two parallel lines (d_p) of the feed network is not changed ($d_p=2$ mm also in the X-band design) since the excess distance between the feed lines decreases the coupling between the lines, thus increases the performance.

The choice between the two substrates, CuFlon and Alumina, can be made by considering the credible process techniques to open lines of copper on the substrate. The advantages and the disadvantages of the substrates can be discussed after remembering the properties of the two together with the Rogers R4003C. Table 3 shows the corresponding substrates and properties.

Table 3. Comparative Substrate Properties.

Substrate	Substrate Thickness (mm)	Relative Dielectric Constant	Line Width of 50 Ω Line (mm)
R4003C	0.508	3.38	1.15
CuFlon	0.254	2.21	0.80
Alumina	0.254	9.96	0.27

Alumina necessitates higher precision process techniques due to its smaller wavelength, thus smaller dimensions. In return, the smaller line width may be an advantage. On the other hand, CuFlon can be processed easier, but if necessary, it cannot be produced in the clean room conditions.

The first choice is CuFlon which is easier to process. If any technical unfeasibility that can be fixed by Alumina occurs, the design is resumed.

The Smith Chart locations for the DGS simulated as a transmission line are also investigated for varying substrate materials. The corresponding structure and the Smith Chart location results for 10 mil and 20 mil CuFlon substrates can be seen in Figure 48.

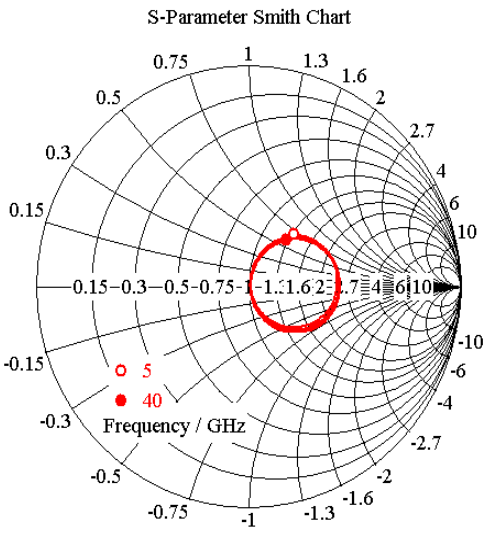


Figure 48.a. Smith Chart Location for CuFlon RS-DGS Normalized to 50Ω , with $h=10$ mil, $w=0.8$, $w_d=1$ mm.

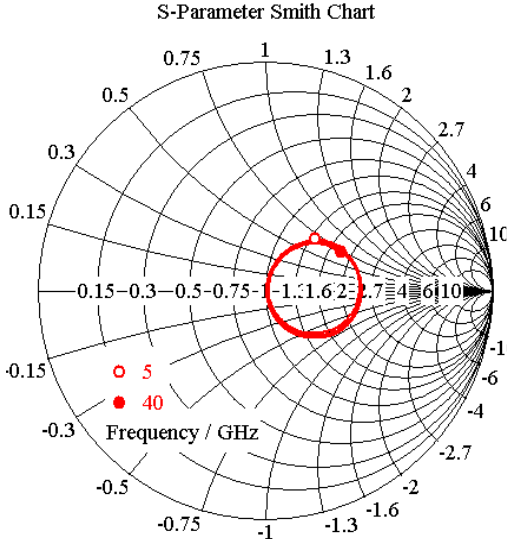


Figure 48.b. Smith Chart Location for CuFlon RS-DGS Normalized to 50Ω , with $h=20$ mil, $w=1.6$, $w_d=2$ mm.

The Smith Chart locations for the Alumina substrate DGS-TL are also simulated. The simulations are carried out for 10 mil substrate thickness. The corresponding results can be seen in Figure 49.

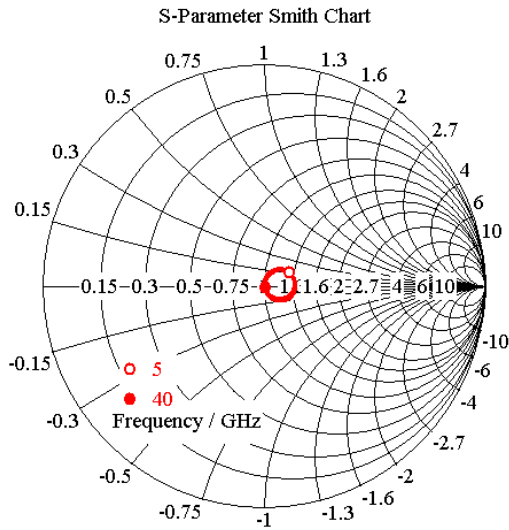


Figure 49.a. Smith Chart Location for Alumina RS-DGS Normalized to 50 Ω , with $h=10$ mil, $w=0.27$, $w_d=0.5$ mm.

The results for the transmission-line simulated DGS using both Alumina and Cufion substrates again show that the structure is a high-impedance structure.

For 10 mil substrates, the line widths are nearly halved, becoming compatible with small defect lengths; and the impedance transformation at 35 GHz becomes possible. Figure shows the magnitude of S_{11} versus the changes in the structure parameters for a T-junction.

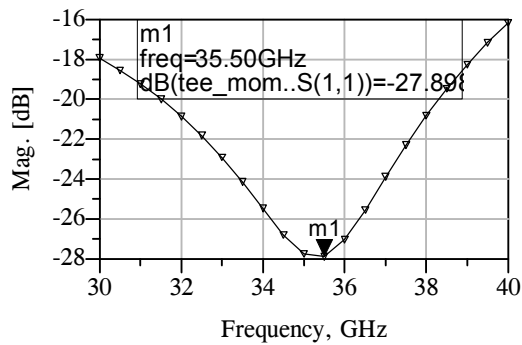


Figure 50.a. S_{11} for DGS T-junction Using CuFlon Substrate of $d=10$ mil, $w=0.8$, $w_d=1.2$, $d=0.05$, $l=0.75$, $d_p=2$ mm.

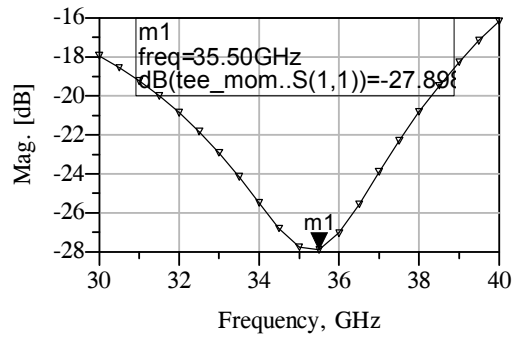


Figure 50. S_{11} for DGS T-junction Using CuFlon Substrate of $d=10$ mil, $w=0.8$, $w_d=1.3$, $d=0.05$, $l=0.65$, $d_p=2$ mm.

The results presented in Figure 50 are the S_{11} results for the T-junction realized by 10 mil CuFlon substrate. The simulations are carried in order to find the best defect length (l), width (w_d), and the defect distance from the junction (d), and the best fit values are chosen as $l=0.75$, $w_d=1.2$, $d=0.05$ mm.

Moving up to the 1 : 4 structure, the device with varying defect length values is simulated and no change is observed in the resonance frequency characteristics. Defect width is varied for 0.75 mm defect length and the corresponding results are plotted in Figure 51.

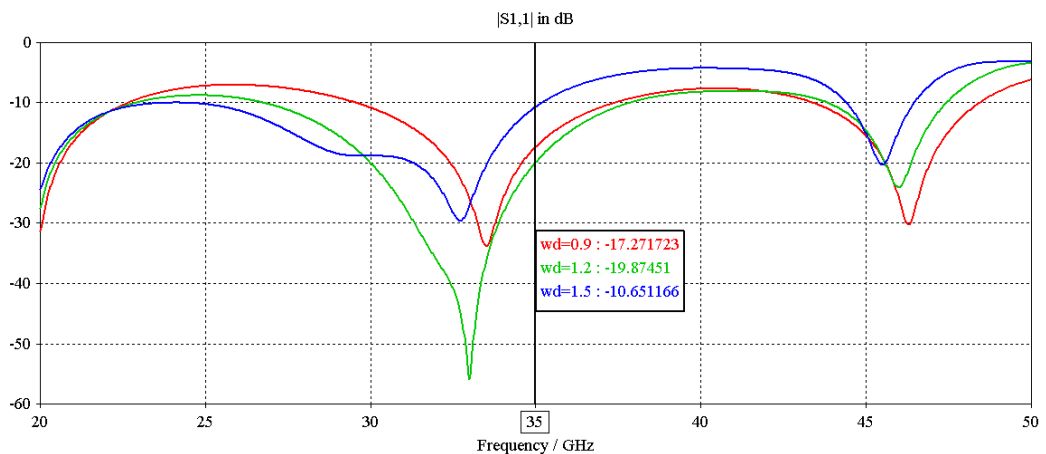


Figure 51. S_{11} for DGS 1 : 4 BFN with CST Using CuFlon Substrate of $d=10$ mil, $w=0.8$, $w_d=0.9:0.1:1.5$, $d=0.05$, $l=0.75$, $d_p=2$ mm with the Second Dielectric & Ground Added Beneath.

The resonance frequency could not be set to 35 GHz, the change in neither defect length nor defect width could make a change in the resonant frequency (See Figure 51).

35 GHz design can also be attempted with Alumina substrate. However, the reasons for the non-ideal design completed by the CuFlon substrate must be questioned first. The examination of the reasons for the unexpectedly wide-band behavior of the DGS BFN may be a good point to start. The novel difference between a standard BFN and a DGS BFN is the defect on the ground. As the number of defects increase, i.e., as the stages of the BFN increases, the band of the structure widens. So, one may claim that the coupling between the defects lead to a wide-band behavior, and this claim can be supported by the designer's route.

Coupling is typically not desired in the design of a feed network. So, the only non-modified variable from the 10 GHz design was the distance between the two parallel lines (d_p) which would better reduce coupling. However, with the curiosity of monitoring the effect of coupling between the defects, change is done, and the result has shown that the cross-coupling between the defects play an important role in the wide-band behavior of the DGS BFN. The structure with its new parameters and the corresponding results can be seen in Figure 52.

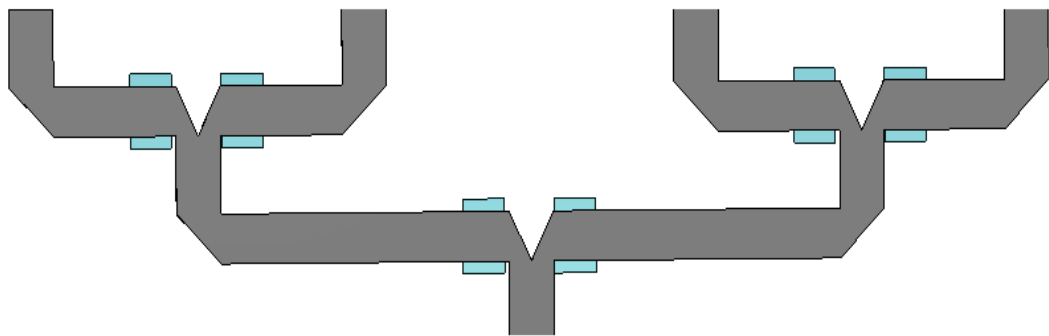


Figure 52.a. DGS 1 : 4 BFN with $w=0.8$, $w_d=1.2$, $l=0.75$, $d=0.05$, $l_0=6$, $d_p=1.25$ mm with the Second Dielectric & Ground Added Beneath.

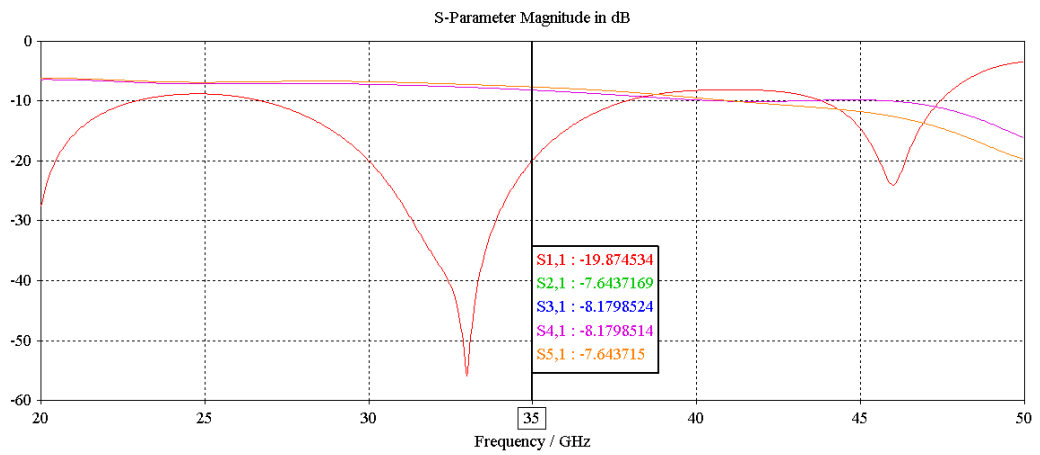


Figure 52.b. S_{11} for the 1 : 4 Structure with $w=0.8$, $w_d=1.2$, $l=0.75$, $d=0.05$, $l_o=6$, $d_p=2$ mm with the Second Dielectric & Ground Added Beneath.

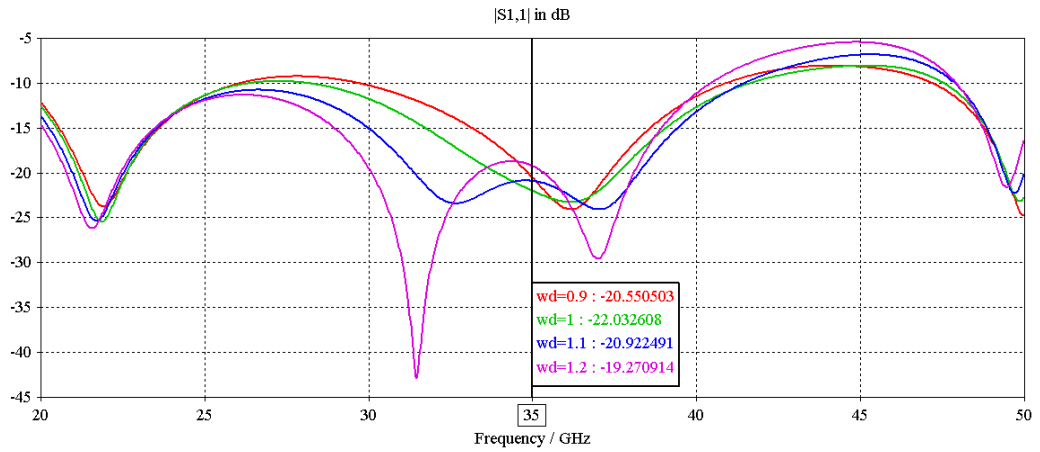


Figure 52.c. S_{11} for the 1 : 4 Structure with $w=0.8$, $w_d=1.2$, $l=0.75$, $d=0.05$, $l_o=6$, $d_p=1.25$ mm with the Second Dielectric & Ground Added Beneath.

The wide-band property seems to be active at the $d_p=1.25$ mm case. So, it can be used in the further design procedure. The change in the second order defect widths is necessary in order to equalize the power at the second and third ports. The corresponding results with the related parameters can be seen in Figure 53.

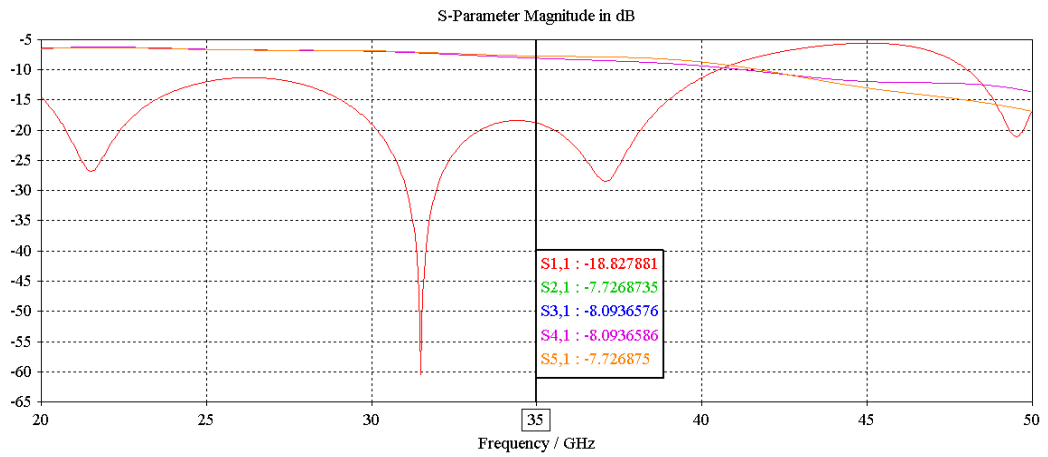


Figure 53.a. S-parameters for the DGS 1 : 4 BFN with $w=0.8$, $w_d=1.2$, $l=0.75$, $d=0.05$, $l_o=6$, $d_p=1.25$, $w_{d2}=1.3$, $w_{d3}=1.1$ mm with the Second Dielectric & Ground Added Beneath.

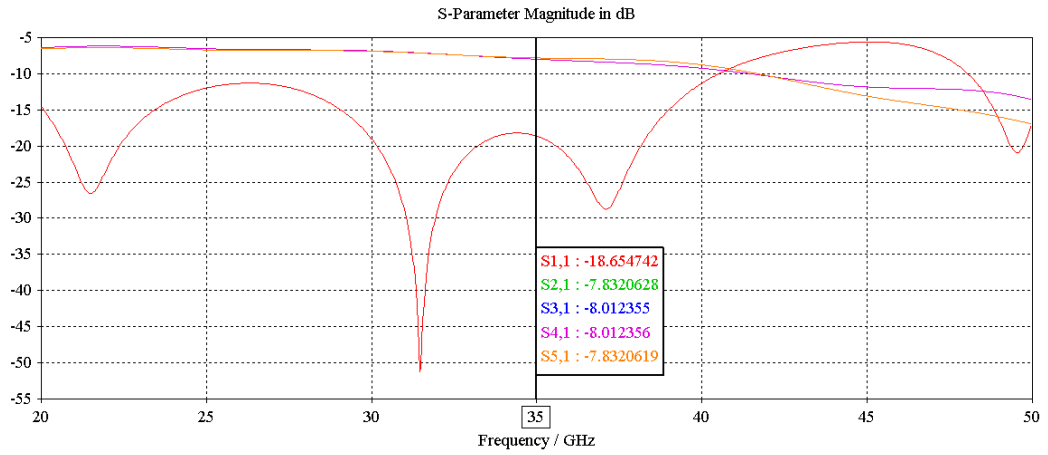


Figure 53.b. S-parameters for the DGS 1 : 4 BFN with $w=0.8$, $w_d=1.2$, $l=0.75$, $d=0.05$, $l_o=6$, $d_p=1.25$, $w_{d2}=1.32$, $w_{d3}=1.08$ mm with the Second Dielectric & Ground Added Beneath.

Referring to Figure 53, impedance match condition can be assured in the 28.5 GHz – 38.5 GHz band. However, at these frequencies, despite the good matching condition, S_{21} & S_{31} (-7.8 & -8 dB respectively) show that radiation loss is a problem at these frequencies (0.8 dB insertion loss). There exists a 0.37 dB difference between the two asymmetric ports (2 & 3, 4 & 5); when the defect widths at these ports are changed as 1.30 to 1.32, and 1.08 to 1.1 the port powers difference becomes 0.17 dB. However, this change requires a precise processing technology which is probably not worth trying. Additional-

ly, phase values of the S-parameters should be checked. Figure 54 shows the S-parameter phase values.

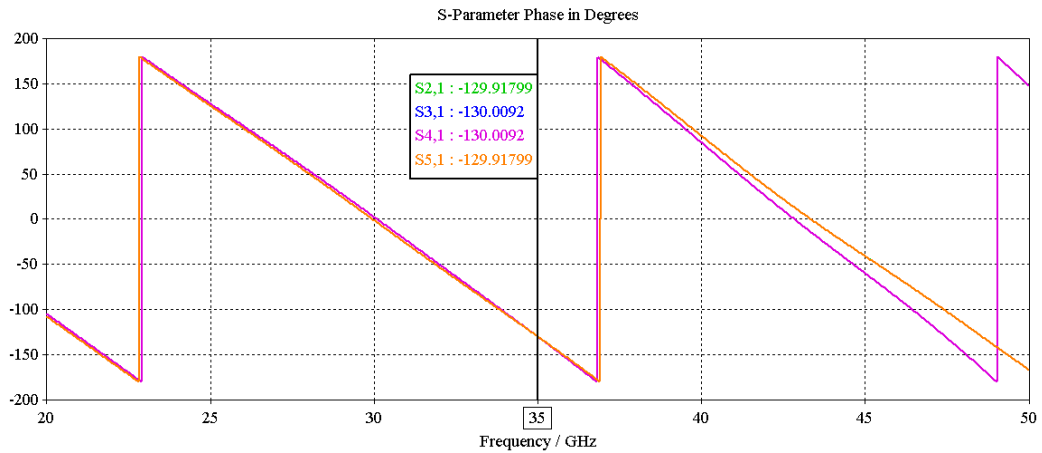


Figure 54. S-parameters Phase Values for the DGS 1 : 4 BFN with $w=0.8$, $w_d=1.2$, $l=0.75$, $d=0.05$, $l_0=6$, $d_p=1.25$, $w_{d2}=1.32$, $w_{d3}=1.08$ mm with the Second Dielectric Added Beneath..

The phase difference between the ports can be ignored in the 28.5 GHz – 38.5 GHz band, so the device can be called as equi-phase.

Owing to the experienced performance of the ADS Momentum on the planar and layered structures, the 35 GHz design is preferred to be simulated with ADS as a final, and awaiting resultant behavior. The corresponding results can be seen in Figure 55. Note that, all the parameters are the same as in the CST design. In both the designs, there exists a substrate of the same thickness, 10 mil, beneath the DGS, and an additional ground exists below the second substrate.

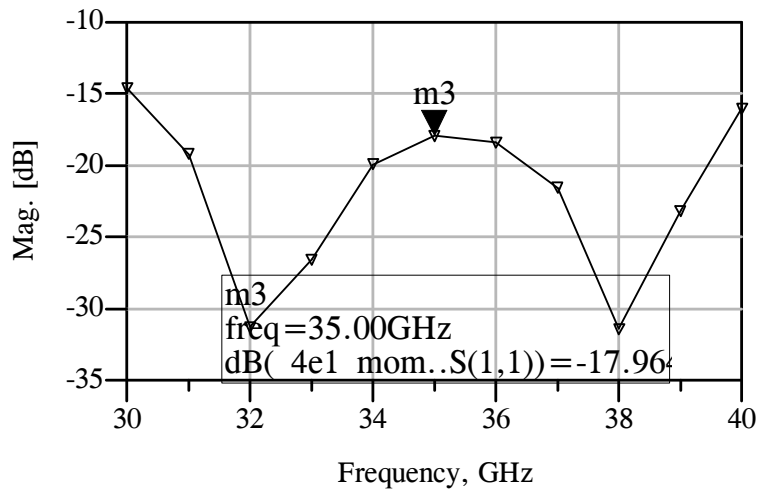


Figure 55.a. Reflection Magnitude Characteristics of the DGS 1 : 4 BFN with $w=0.8$, $w_d=1.2$, $l=0.75$, $d=0.05$, $l_0=6$, $vv=1.25$, $w_{d2}=1.3$, $w_{d3}=1.1$ mm with the Second Dielectric Added Beneath.

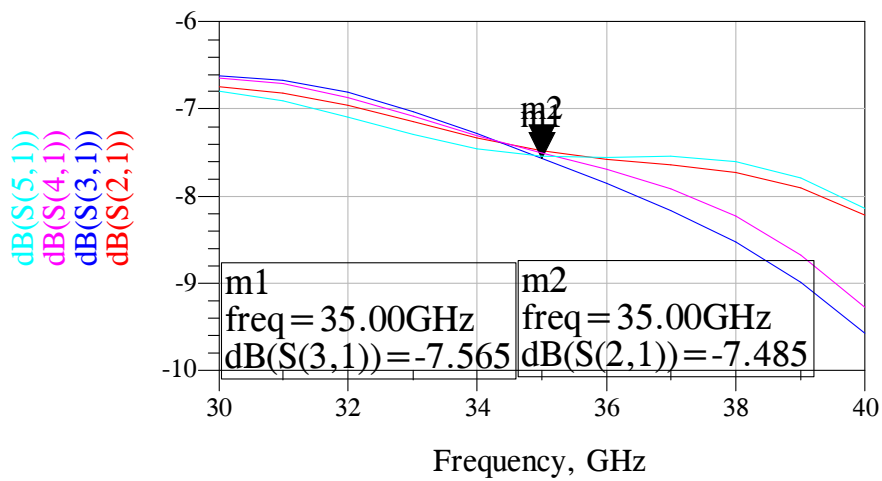


Figure 55.b. Transmission Magnitude Characteristics of the DGS 1 : 4 BFN with $w=0.8$, $w_d=1.2$, $l=0.75$, $d=0.05$, $l_0=6$, $vv=1.25$, $w_{d2}=1.3$, $w_{d3}=1.1$ mm with the Second Dielectric Added Beneath.

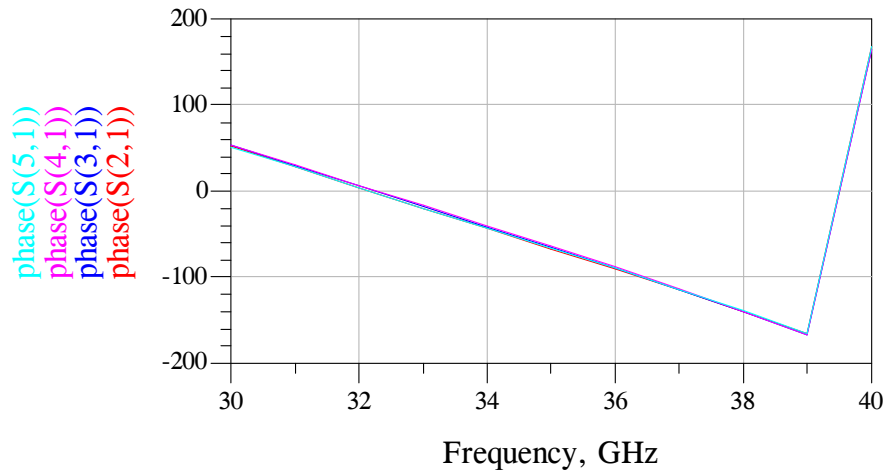


Figure 55.c. Transmission Phase Characteristics of the DGS 1 : 4 BFN with $w=0.8$, $w_d=1.2$, $l=0.75$, $d=0.05$, $l_0=6$, $vv=1.25$, $w_{d2}=1.3$, $w_{d3}=1.1$ mm with the Second Dielectric Added Beneath.

Considering the results of ADS Momentum, Figure 55, it can be said that both the two solvers state that the device is matched, and the phases are equal in the 28.5 GHz – 38.5 GHz band. However, the transmitted power level is still low. It would be convenient to calculate the total loss of the device, and then compare it with a standard BFN which is again designed by ADS Momentum, using 10 mil Cufion substrate at 35 GHz.

$$P_{loss\ dB-DGS\ BFN} = 10 \times \log \left(\frac{1}{\left(10^{\frac{S_{11}}{10}} + 10^{\frac{S_{21}}{5}} + 10^{\frac{S_{31}}{5}} \right)} \right) = 10 \times \log \left(\frac{1}{0.72} \right)$$

$$= 10 \times \log (1.38) = 1.4\ dB\ at\ 35\ GHz$$

For the standard case, S-parameters simulation results are given as $S_{11}=-29.43$ dB, $S_{21}=S_{51}=-6.48$ dB, $S_{31}=S_{41}=-6.74$ dB which corresponds to a loss of 0.58 dB. So, this comparison shows that the radiation loss due to the defect is active at the millimeter-wave frequencies.

CHAPTER 5

CONCLUSIONS

The increasing demands of the microwave applications necessitate the design and implementation of novel and target oriented components instead of the standard applications. The availability of such components boots the flexibility of the designers.

This thesis presents a new transmission line design using RS-DGS instead of the commonly used types. This design technique offers the advantages of space saving and increased impedance range. Consequently, sensitivity to production tolerance decreases. The required precision of the production technology for a 70.7Ω line width is the same as that of 50Ω line width of the microstrip line. As an example, using Rogers R4003C substrate, a $50 \mu\text{m}$ precision is sufficient since the 50Ω line width is 1.15 mm , however when the 70.7Ω line is used, the precision requirement increases since the corresponding line width decreases to 0.66 mm .

Similarly, for CuFlon substrate 0.8 mm and 0.47 mm are the line widths for the 50Ω and 70.7Ω line impedances, respectively. Apart from these line-width restrictions, the discontinuity of the line widths between different characteristic impedances are also another factor playing an important role in the design considerations which are also eliminated by the use of the DGS.

The space saving property of the DGS is also widely known and used concerning the minimal, and compact designs [13-16]. It I shown that implementation of the RS-DGS on the T-junction has resulted in a length reduction of 33% compared with the standard approach. The length of the RS-DGS depends on the distance of the defect from the junction (d). The length of the defect (l) at a desired frequency and the defect width (w_d) are used to satisfy the impedance matching.

Similar RS-DGS structures are also used in the BFNs, but since the distance between the two adjacent ports of a BFN is controlled by the air wavelength, impedance matching circuitry is not a restricting component for the BFN case.

Moreover, implementation of the RS-DGS to the BFNs was not reported before in the open literature. The same design parameters of the T-junction are applicable to the BFN design: d , l , w_d . However, in the BFN case, w_d is the decisive component predominantly controlling the wideband behavior. Additionally, the distance between the two stages (d_p) is also important for band-broadening. If a wideband design is desired, which is the most advantageous part of a DGS BFN, one must also adjust d_p . While adjusting these parameters, the change can be made as in the standard case, i.e., as the frequency increases, the lengths decrease, this is true for all the d , l , and d_p values.

The usage of the DGS with the BFN also offers a compact design with all 50Ω lines on the line side. Apart from these advantages, DGS BFN starts to be disadvantageous as the frequency increases due to the increasing loss coming from the radiation of the defects. The BFN design at 35 GHz shows that it is not possible to use the DGS approach at the millimeter-wave frequencies, or if desired, the designer should be aware of the radiation losses.

Considering the RS-DGS studies, many applications have been introduced up to now. However, there is still more to do at this context. So it would be convenient to conclude with the future work.

5.1 Future Work

The RS-DGS transmission line is a new concept which can be introduced as a new form of a microstrip line, or as an inclined coplanar line. The parameterization and the circuit modeling of the line would be the first goal.

The cascade application of the defects was realized before only for the EBG structures which are also active or passive in a band of frequencies. The usage of the defects in an antenna feed network is also cascade, and an analogy can be formed between the band-select properties of the EBGs and the wideband properties of a feed network. Furthermore, studies associating the radiation from the defects and the behavior of the microwave network can be conducted. There exists some studies focusing on the radiation from the defects of a PBG [35], but these studies only focus on the radiation from the

PBG, but do not associate these results with the behavior of the network. Since no studies exist in this area, studies correlating the radiation from the defects to the performance of device would be experienced, and if the correspondence is discovered, it would broaden the horizons in this area.

Additionally, the reconfigurability of the power division ratio, or basically the impedance value can also be realized with the implementation of switches placed on the ground. One implementation may be the insertion of switches between two defects placed as one inside the other, and the impedance keeps its value in accordance with the active defect.

Taking a general look at the DGS research and applications being conducted all over the world, the rectangular-shaped defect studies make up a small portion of the overall. The research is commonly focused on the filter applications. The examination of novel DGSs would be a good research topic and would be exceptional if succeeded.

REFERENCES

- [1] Ahn, D.; Park, J.-S.; Kim, C.-S.; Kim, J.; Qian, Y.; Itoh, T., "A design of the low-pass filter using the novel microstrip defected ground structure," *Microwave Theory and Techniques, IEEE Transactions on* , Vol.49, no.1, pp.86-93, Jan 2001.
- [2] C. S. Kim, J. S. Park, D. Ahn, and J. B. Lim, "A novel 1-D periodic defected ground structure for planar circuits," *IEEE Microw. Wireless Compon. Lett.*, Vol. 10, no. 4, pp. 131–133, Apr. 2000.
- [3] Liu, H., Z. Li, and X. Sun, "Compact defected ground structure in microstrip technology," *Electron. Lett.*, Vol. 41, No. 3, pp. 132–134, 2005.
- [4] Mandal, M. K. and S. Sanyal, "A novel defected ground structure for planar circuits," *IEEE Microwave Compon. Lett.*, Vol. 16, No. 2, pp. 93–95, 2006.
- [5] J.-S. Lim, C.-S. Kim, Y.-T. Lee, D. Ahn, and S. Nam, "Design of lowpass filters using defected ground structures and compensated microstrip line", *Electron Lett*, Vol. 38, pp. 1357–1358, 2002.
- [6] Karmakar, N.C.; Roy, S.M.; Balbin, I., "Quasi-static modeling of defected ground structure," *Microwave Theory and Techniques, IEEE Transactions on* , Vol.54, no.5, pp. 2160-2168, May 2006.
- [7] Easter, B., "The Equivalent Circuit of Some Microstrip Discontinuities," *Microwave Theory and Techniques, IEEE Transactions on* , Vol.23, no.8, pp. 655-660, Aug 1975.
- [8] R. Garg and I. J. Bahl, "Microstrip discontinuities," *Int. J. Electron.*, Vol. 45, no. 1, pp. 81–87, 1978.
- [9] Thomson, A.F.; Gopinath, A., "Calculation of Microstrip Discontinuity Inductances," *Microwave Theory and Techniques, IEEE Transactions on*, Vol.23, no.8, pp. 648-655, Aug 1975.

- [10] Hamad, E. K. I., A. M. E. Safwat, and A. S. Omar, "Controlled capacitance and inductance behaviour of L-shaped defected ground structure for coplanar waveguide," *IEEE Proc. – Microwave Antennas Propag.*, Vol. 152, No. 5, pp. 299–304, 2005.
- [11] J.-S. Lim, C.-S. Kim, Y.-T. Lee, D. Ahn, and S. Nam, "A spiral-shaped defected ground structure for coplanar waveguide," *IEEE Microw. Wireless Compon. Lett.*, Vol. 12, no. 9, pp. 330–332, Sep. 2002.
- [12] C. S. Kim, J. S. Park, D. Ahn, and J. B. Lim, "A novel 1-D periodic defected ground structure for planar circuits," *IEEE Microwave Guide Wave Lett.*, Vol. 10, pp. 131–133, Apr. 2000.
- [13] Sung, Y. J., C. A. Ahn, and Y. S. Kim, "Size reduction and harmonic suppression of rat-race hybrid coupler using defected ground structure," *IEEE Microwave and Wireless Components Letter*, Vol. 14, No. 1, 7–9 Jun. 2004.
- [14] J. S. Lim, H. S. Kim, J. S. Park, D. Ahn, and S. Nam, "A power amplifier with efficiency improved using defected ground structure," *IEEE Microwave Wireless Compon. Lett.*, Vol. 11, pp. 170–172, Apr. 2001.
- [15] J. S. Lim, J. S. Park, Y. T. Lee, D. Ahn, and S. Nam, "Application of defected ground structure in reducing the size of amplifiers," *IEEE Microwave Wireless Compon. Lett.*, Vol. 12, pp. 261–263, July 2002.
- [16] Lim J-S, Jeong Y-C, Ahn D, Lee Y-T, Cho H and Nam S, "Size-reduction and harmonic-rejection of microwave amplifier using spiral-defected ground structure," *European Microwave Conf.*, Vol 3, pp. 1421–4, 2003.
- [17] J.-S. Lim, S.-W. Lee, C.-S. Kim, J.-S. Park, D. Ahn, and S. Nam, "A 4:1 Unequal Wilkinson Power Divider," *IEEE Microwave and Wireless Components Letters*, Vol. 11, no. 3, pp. 124 - 126, Mar. 2001.
- [18] Chang, C.-P., C.-C. Su, S.-H. Hung, Y.-H. Wang, and J.-H. Chen, "A 6 : 1 unequal wilkinson power divider with EBG CPW," *Progress In Electromagnetics Research Letters*, Vol. 8, pp. 151-159, 2009.

- [19] J.-S. Lim, C.-S. Kim, J.-S. Park, D. Ahn, and S. Nam, "Design of 10dB 90° branch line coupler using microstrip line with defected ground structure," *IEEE Electronics Letters*, vol. 36, no. 21, pp. 1784–1785, Oct. 2000.
- [20] W.-L. Chen, G.-M. Wang, Y.-N. Qi, and et al., "A novel wide stopband PBG structure with fractal features and its application to the design of microstrip low-pass filter," *ISAPE2006*, Vol. 1, pp. 292–295, 2006.
- [21] H.-W. Liu, X.-W. Sun, and Z.-F. Li, "A low-pass filter of wide stopband with a novel multilayer fractal photonic bandgap structure," *Microwave Opt Tech Lett.*, Vol. 40, 2004.
- [22] I.K. Kim, N. Kingsley, M. Morton, et al., "Fractal-shaped microstrip coupled-line bandpass filters for suppression of second harmonic," *IEEE Trans Microw Theory Tech.*, Vol. 53, pp. 2943–2948, 2005.
- [23] G.L. Matthaei, "Short-step Chebyshev impedance transformers," *IEEE Trans Microwave Theory Tech.*, Vol. 14, 372–383, 1966.
- [24] J.W. Bandler, "Optimum noncommensurate stepped transmission line transformers," *Electron Lett.*, Vol. 4, 1968.
- [25] Y.L. Chow, K.L. Wan, "A transformer of one-third wavelength in two sections—For a frequency and its first harmonic," *IEEE Microwave Wireless Compon Lett.*, Vol 12, pp. 22–23, 2002.
- [26] C. Caloz and T. Itoh, "Multilayer and anisotropic planar compact PBG structures for microstrip applications," *IEEE Trans. Microw. Theory Techn.*, vol. 50, no. 9, pp: 2206–2208, Sept. 2002.
- [27] C. Caloz, C.C. Chang, and T. Itoh, "A novel anisotropic uniplanar compact photonic band-gap (UC-PBG) ground plane," *The 31st Eur Microwave Conf, London 2*, pp. 185–187, 2001.
- [28] Kordzadeh, A. and F. Hojatkashani, "A new reduced size microstrip patch antenna with fractal shaped defects," *Progress In Electromagnetics Research B*, Vol. 11, pp. 29–37, 2009.

- [29] T. Tanaka, K. Kusoda, and M. Aikawa, "Slot-coupled directional couplers on both-sided substrate MIC and their applications," *Electron. Commun. Jpn.*, vol. 72, no. 3, pt. 2, 1989.
- [30] M.-F. Wong, V. F. Hanna, O. Picon, and H. Baudrand, "Analysis and design of slot-coupled directional couplers between double-sided substrate microstrip lines," *IEEE Trans. Microw. Theory Tech.*, Vol. 29, no. 12, pp. 2123-2129, 1991.
- [31] A. M. Abbosh, and M. E. Bialkowski, "Design of compact directional couplers for UWB applications," *IEEE Trans. Microw. Theory Tech.*, Vol. 55, no. 2, pp. 189-194, Feb. 2007.
- [32] A. M. Abbosh, "A compact UWB three-way power divider," *IEEE Microwave and Wireless Compon. Lett.*, Vol. 17, No. 8, Aug. 2007.
- [33] J.-S. Lim, S.-W. Lee, C.-S. Kim, J.-S. Park, D. Ahn, and S. Nam, "A 4:1 Unequal Wilkinson Power Divider," *IEEE Microwave and Wireless Components Letters*, vol. 11, no. 3, pp. 124 - 126, Mar. 2001.
- [34] Chang, C.-P., C.-C. Su, S.-H. Hung, Y.-H. Wang, and J.-H. Chen, "A 6 : 1 unequal wilkinson power divider with EBG CPW," *Progress In Electromagnetics Research Letters*, Vol. 8, pp. 151-159, 2009.
- [35] N. Shino and Z. Popovic', "Radiation from ground-plane photonic bandgap microstrip waveguide," in *IEEE MTT-S Int. Microwave Symp. Dig.*, pp. 1079-1082, 2002.